# MIXING CONTROL IN SUPERSONIC RECTANGULAR JETS USING PLASMA ACTUATORS

A THESIS

Presented in Partial Fulfillment of the Requirements for

Graduation with Distinction in the

Department of Mechanical Engineering at

The Ohio State University

By

Robert M. Snyder

*******

The Ohio State University

March 2007

# ABSTRACT

The flow through the exhaust nozzle of a jet engine has been of crucial importance in aerospace applications over the past several decades. A variety of modifications can be made to the nozzles of high-speed jet engines to increase or decrease mixing between the exiting flow and the ambient air; including adding tabs, chevrons, or actuators. Localized arc filament plasma actuators (LAFPA) developed in the Gas Dynamics and Turbulence Laboratory at The Ohio State University have both high amplitude and bandwidth and are suitable for active control of high-speed, high Reynolds number flows. These actuators were implemented on a rectangular nozzle in order to optimize the efficiency of mixing enhancement between the jet and the ambient air. Actuators were tested for a Mach 2.0 flow over a wide range of forcing frequencies and the effects were evaluated using flow visualization techniques. Results show the effects of forcing frequency and other parameters on the development of large-scale structures within the flow. Flow visualization testing over a broad range of forcing frequencies and duty cycles revealed the presence of large coherent structures and thus most favorable mixing enhancement in the 6-8 kHz ($St_F$ = 0.15-0.2) range. The m = ± 1 (flapping) mode produced a clear pattern of alternating structures within the aforementioned frequency band. It was also observed that the effect of varying duty cycle within this frequency range has little effect on the control authority.

# ACKNOWLEDGEMENTS

I would like to thank Dr. Samimy for introducing me to the opportunities available in undergraduate research and allowing me to pursue research at the Gas Dynamics and Turbulence Lab (GDTL). I would also like to acknowledge Jeff Kastner for working closely with me throughout the experimental process, in addition to the countless discussions of theory and experimental technique. I would also like to thank Jin-Hwa Kim for all the time spent helping me complete tests accurately and professionally. Lastly, I am grateful for the additional advice given to me from other members of GDTL, including Jesse Little and Edgar Caraballo.

# TABLE OF CONTENTS

# LIST OF FIGURES

# 1. Introduction

Projects conducted by the research teams at the Gas Dynamics and Turbulence Lab (GDTL) at The Ohio State University encompass a broad range of technical issues in the fields of gas dynamics, flow control, and propulsion. These projects are primarily funded by companies and agencies with specific interests in the study of flow behavior, such as NASA and the Air Force Research Laboratory.

A major focus of the team at the GDTL at The Ohio State University is on the control of high-speed free jets. The most common examples of this application can be seen in the exhaust flow of aircraft engines. Axisymmetric, or circular, jets are found on most common commercial and military aircraft. This study, however, focuses primarily on the control of flows through a nozzle of rectangular geometry. The rectangular nozzles being considered in this project are of significant importance in high performance stealth military aircraft. By enhancing mixing in the shear layer trailing the nozzle, the hot exhaust from the jet is able to mix more quickly with cool ambient air. Increasing this mixing removes a significant amount of the heat signature of the jet, thus increasing stealth capabilities. Reducing the mixing behind the jet has the effect of drastically cutting down the noise generated by the engine. Research in this field offers a range of positive effects with both military and commercial applications. A schematic of the rectangular jets being considered in this project can be seen in Figure 1 below.

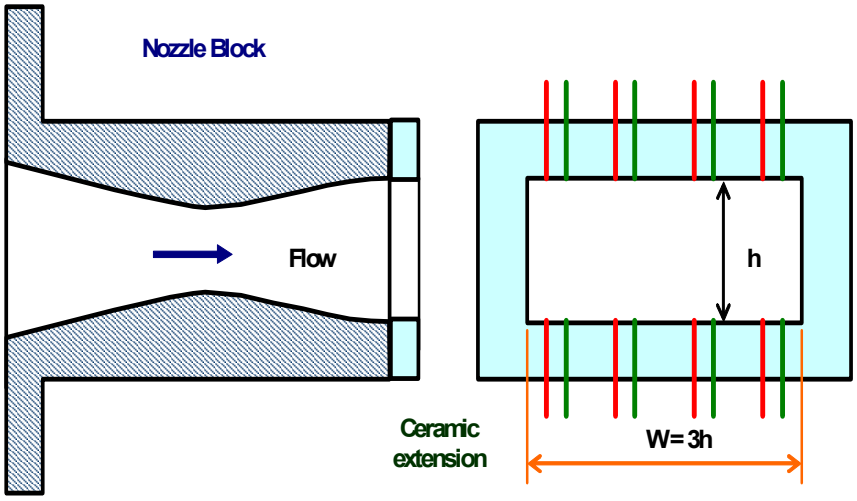


Figure 1. Rectangular nozzle concept.

Modifications can be made to the nozzles of high-speed jet engines to increase or decrease mixing between the exiting flow and the ambient air. Several methods for flow manipulation by geometrical modifications to the nozzle exit have been explored, including tabs, chevrons, and other trailing edge modifications. These forms of passive control are always present within the flow, enhancing mixing, but also inducing negative effects such as thrust loss due to blockage. Active control differs from passive control in that energy is added to the flow, rather than simply modifying the nozzle geometry. The benefit of this method is that active control has the ability to be turned on and off. This not only reduces negative effects associated with inserting geometrical modifications into the flow, but also allows the user to utilize the manipulation only when necessary.

The majority of prior research using plasma actuators has focused on circular (axisymmetric) jets. For this reason, the challenge of this study comes from the rather unpredictable nature of the phenomenon being observed. Without a previous knowledge

base, little can be expected or assumed by implementing plasma actuators on a nozzle with rectangular geometry.

This thesis details the development and implementation of localized arc filament plasma actuators on a nozzle of rectangular geometry. Initial flow visualization studies have been completed, yielding some defining characteristics of the forcing effect on high-speed flows. Future work in the field is intended for the completion of a Master of Science degree at The Ohio State University.

# 2. Background

## *2.1 Introduction*

In order to conduct research in the field of free jet control, an extensive knowledge basis has to first be developed in the areas of gas dynamics, control techniques, and experimental methods. At least an introductory working knowledge of each of these fields must be acquired in order to examine the effects of active control of high-speed flows. The following subsections discuss the principles of gas dynamics, flow control and introductory descriptions of control methods required for this type of research.

## *2.2 Gas Dynamics*

Through prior testing on axisymmetric nozzles at the facility, it was seen that the manipulation of jet instabilities yielded significantly increased mixing for axisymmetric jets (Samimy et. al. 2004, 2007a & 2007b). In order to effectively attempt a similar manipulation of instabilities, the first step required is to determine the forcing frequency required to excite such instability. By observing the degree of mixing enhancement that results from various forcing frequencies, an approximation of the preferred frequency of the jet can be made. An estimation of the preferred frequency of the jet can be made based on previous experimentation and through the use of the Strouhal number. The Strouhal number represents a non-dimensional frequency and can be calculated as follows:

$$St = \frac{f \cdot h}{U_j} \tag{1}$$

where $f$ is the frequency of the flow instability in Hertz, $h$ is nozzle height in meters, and $U_j$ is jet velocity in meters per second. By using Strouhal number as opposed to

frequency, the results obtained can be scaled to compare with those obtained in other labs. Assuming a Strouhal number of 0.25 (Olsen et. al. 2003), a common experimentally derived preferred Strouhal number for rectangular jets; the equation presented above could be used to solve for frequency. The nozzle height is held fixed at 0.0127 meters (0.5 inches). Jet velocity can be derived using the definition of Mach number. Mach number represents the ratio of jet velocity to the speed of sound. In order to determine the speed of sound for a particular flow, the temperature of the flow must first be calculated. Given the temperature conditions present within the stagnation chamber, as well as the design Mach number of the jet, the following equation can be used to calculate flow temperature (Anderson 2004):

$$\frac{T_o}{T} = 1 + \frac{\gamma - 1}{2} M^2 \tag{2}$$

where $T_o$ is stagnation temperature in Kelvin, $T$ exit temperature of the flow in Kelvin, $\gamma$ represents the specific heat ratio (1.4 for air), and $M$ is the given design Mach number. Once temperature is known, the following equation can be used to find the speed of sound ($c$) at this temperature (Anderson 2004):

$$c_j = \sqrt{\gamma R T} \tag{3}$$

where $R$ is the gas constant for the fluid (287 J/kg-K for air), and $c$ represents the speed of sound in meters per second. With the determined speed of sound and given Mach number, the definition of Mach number can be used to find the flow velocity, as follows:

$$M = \frac{U_j}{c_j} \quad \Rightarrow \quad U_j = M c_j \tag{4}$$

where $U_j$ is jet velocity in meters per second. Lastly, with this flow velocity, the definition of Strouhal number can be rearranged to solve for preferred frequency, based on the experimentally determined Strouhal number of 0.25:

$$St = \frac{f_p h}{U_j} \quad \Rightarrow \quad f_p = \frac{U_j St}{h} \tag{5}$$

where $f_p$ is the preferred frequency of the flow in Hertz. Using the known Mach number of 2.0 and calculated local speed of sound ($c_j$ = 251.34 m/s), the jet velocity ($U_j$ = 502.68 m/s), and therefore preferred frequency, could be calculated. This procedure yielded an estimated preferred frequency of 9900 Hz.

This gives an estimation of the frequency to operate the plasma actuators when mixing enhancement is desired. Since this is just an estimate, a range of frequencies should be tested to find a frequency for optimum performance. This estimation allows reduction in the range of frequencies considered, thus decreasing the amount of tests required. In the present work, the range tested is roughly 2-20 kHz. More frequencies are tested around the predicted preferred frequency determined from the preceding method. With this preferred frequency, a narrower band of frequencies surrounding this preferred value can be explored to ensure that the optimum forcing frequency is found.

### *2.3 Control Techniques*

There are two main categories of manipulation techniques to control jet dynamics: direct excitation of jet instabilities, and imparting longitudinal (streamwise) vortices into the mixing layer of the jet. Streamwise vortices can be thought of as structures within the flow that swirl around an axis parallel to the jet axis. These vortices give rotational spin to the air mass exiting the nozzle. Due to the fact that streamwise vortices are not appreciably affected by compressibility, they appear to be an effective way of increasing

mixing with ambient air downstream of the nozzle exit. For low-speed applications, jet instability excitation and streamwise vorticity generation have been successfully used. For high-speed applications, however, the lack of high amplitude and high bandwidth actuators has made the utilization of jet instability excitation difficult (Samimy et al. 2004). The localized arc filament plasma actuators can be used for both vorticity generation and instability excitation in both high-speed and low-speed applications, where previous actuators could not. In the present study, active control using LAFPA will be applied, making both vorticity generation and instability excitation viable alternatives.

Generating streamwise vorticity in the flow has been proven to be fairly successful for both low-speed and high-speed jet engines, and has been somewhat easier to implement than forcing instabilities, but not as effective (Kim and Samimy 1998, 1999). For geometrical modifications (or passive control), which lack frequency control, streamwise vorticity generation is the only real alternative. A principal method for establishing a streamwise vorticity is by setting up a spanwise pressure gradient in front of a surface protrusion, such as a tab. Other similar experiments have reinforced the theory of spanwise pressure gradients being the main source of streamwise vorticity, thus increasing mixing or reducing noise. Tabs have been researched thoroughly, the results of which are favorable except for the aforementioned negative blockage effects and associated thrust losses. The proposed plasma actuators allow all the positive effects of tabs, but with the ability to be readily turned on and off, reducing the thrust loss.

Alternatively, there are two main instabilities within the jet that can be manipulated: shear layer instability at the nozzle exit, and the jet column instability, amplified near the end of the potential core. Excitation at certain Strouhal numbers (normalized frequency) leads to an increase in shear layer growth, turbulence intensity,

and high amplitude tones in the acoustic field. Excitation at various amplification rates has varying effects on mixing enhancement and noise reduction (Samimy et al. 2007a&b). The utilization of plasma actuators permits the use of this technique due to their high amplitude and bandwidth. Control of instabilities has a profound effect on the mixing layer and will be the main source of manipulation throughout this project. Once the specific instabilities are found, they can be actively controlled to produce desirable effects.

### *2.4 Actuators*

Active control of high-speed jets has been difficult due to the lack of actuators with the appropriate characteristics. Attributes required for handling such flows are high amplitude, high bandwidth, phase control, and small size but with sufficient robustness to withstand the harsh environment. Localized arc filament plasma actuators (LAFPA) developed in the Gas Dynamics and Turbulence Laboratory at The Ohio State University have all these properties, making them suitable for active control of high-speed, high Reynolds number flows (Samimy et. al. 2004 & 2007a). An actuator is formed by placing two electrodes in close proximity and sending a high voltage (~8 kV) across them, which then ionizes the air between them, producing an arc filament discharge. This voltage is supplied by a high voltage D.C. power supply. The supply of the high voltage to an actuator is controlled by a high-voltage transistor switch. The frequency of the actuator is controlled by the pulsating rate to the switch. The actuator system schematic, developed within the GDTL, can be seen in the Figure 2 below.

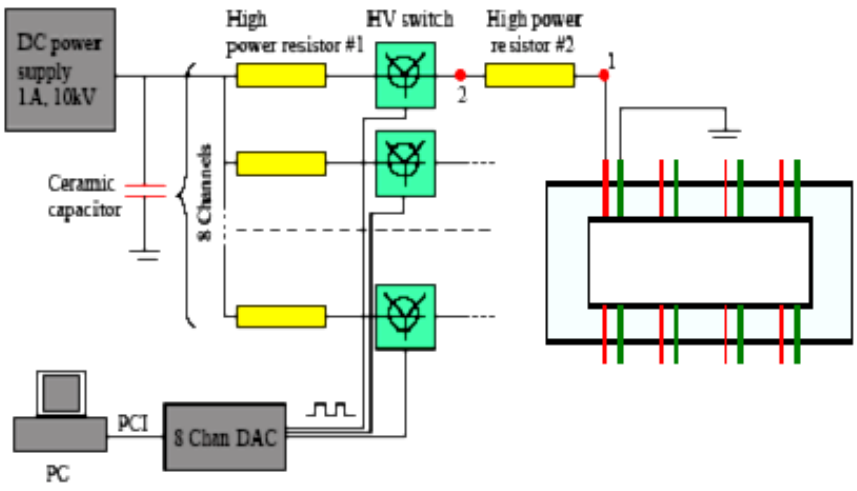


Figure 2. Plasma actuator system schematic.

As this schematic shows, there will be eight actuators used in this experiment, requiring sixteen electrodes. These electrodes alternate between ground and high-voltage. The arc filament produced between electrodes forms plasma that acts as a thermal/pressure perturbation placed within the flow. These concentrated high temperature regions incite the formation of large-scale structures in the flow. These actuators are placed just upstream of the exit of the nozzle. Plasma actuators allow both frequency and phase control, thus making vorticity generation and instability manipulation possible. Plasma actuators also have very low power consumption, requiring only about 1% of the power of the jet flow.

# 3. Experimental Techniques

## *3.1 Introduction*

Several experimental methods exist to determine qualitatively or quantitatively the resultant degree of mixing due to forcing. Several experimental techniques are currently in use at GDTL, including flow visualization, pressure measurements, particle image velocimetry, schlieren imaging, and acoustic measurements. The following will describe the principle techniques employed throughout this study and will detail the nature of each technique.

## *3.2 Flow Visualization*

The primary method used for comparing forced cases will be planar flow visualization of laser light scattered by condensed particles within the jet's mixing layer. The presence of condensation is a direct result of the degree of mixing between the jet and the ambient air. A laser sheet is formed using a Spectra Physics 10 Hz pulsed Nd:YAG laser operating at a wavelength of 532 nm (green laser light). This laser actually utilizes fused silica that produces light at a wavelength of 1064 nm. A Harmonic Crystal within the laser converts the wavelength to 532 nm, making the light green and visible. The laser light is then steered from the laser into the test chamber by mirrors. Once inside the chamber, the beam is passed through a cylindrical lens that spreads out the beam into a sheet. The beam is also passed through a spherical lens that focuses the spread from the cylindrical lens into a thin sheet. This sheet can be used to illuminate streamwise or cross-stream sections of the jet's mixing layer. Laser light is then scattered by condensed particles within the flow to create flow images. The images formed by the laser sheet are captured using a Princeton Instruments Pixis 400 camera with a Nikon

Zoom Nikkor 70-300mm lens. The frequency of laser firing is significantly higher than the rate at which the camera is acquiring images. This ensures that when an image is recorded, the laser will be on and therefore structures will be visible. Flow visualization allows quick qualitative analysis of the amount of mixing and control authority by visual comparison between forcing cases and a baseline case with no control. A variety of Mach numbers and actuator excitations can be produced through the provided equipment to find the optimum levels of operation.

As previously mentioned, flow visualization depends primarily on the amount of water vapor condensed when entrained by the dry and cold jet. Due to the lowered exit temperature of a supersonic jet, the increased temperature gradient allows for moisture within room temperature ambient air to cool more readily and subsequently condense as it is entrained. The amount of condensation present within the shear layer provides an indication not only of the amount of mixing, but also of the size of the structures formed. For flow visualization to be effective, the temperature gradient between the flow and ambient air must be appreciable, as does the humidity. Therefore, this testing method depends largely on the weather conditions for any given day of testing. It is therefore considered good practice to complete all tests for a given battery of testing on the same day to ensure consistency between images. Ideally, condensation should be visible near the nozzle exit for acceptable flow visualization images. For condensation to appear further downstream indicates a lack of proper testing conditions for the given design Mach number of the jet. To remedy this problem, a higher Mach number jet can be introduced in order to further lower the exit temperature of the jet and provoke increased condensation. For a given tank stagnation temperature of 10°C, increasing the Mach

number of the flow from 1.3 to 2.0 reduces the exit temperature from -61.5°C to -115.8°C. Switching to a higher speed flow does therefore allow condensation to become more visible. However, with too much humidity, condensation can also form on the extension itself, leading to unwanted plasma arcing between electrodes. A balance must be found between a low humidity that will prevent condensation and a high humidity that may allow condensation to form on the extension.

Lastly, this system also has the capability to be phase-locked with actuator firing to better educe the large-scale structures generated by forcing. With these structures much more pronounced, qualitative analysis between forcing cases can be made much more readily. Even without phase locking, averaging of random images can be used to produce an average image for each forcing frequency. Although this method can be effective in showing the differences between forced cases, phase locking ensures the maximum performance of each frequency can be distinctly discerned.

### *3.3 Particle Image Velocimetry*

Particle image velocimetry (PIV) is also frequently used to analyze flows. Similar to flow visualization, this technique is based on collecting images that capture laser light scattered off of particles within the flow. Rather than relying on condensation, however, PIV is based on particles seeded into the jet flow as well as co-flow surrounding the jet. This technique allows spatial information to be collected, but does not record any sort of time history. Other techniques, such as the aforementioned pressure transducer measurements, exist in which a time history can be recorded, but spatial information is lost unless additional probes are placed within the flow. Doing so,

however, requires additional obstructions to be positioned within the flowfield and can influence the results.

The basis of PIV is the collection of multiple images of the flow field. Two images are recorded in rapid succession (approximately 2 μsec) with a CCD camera. The movement of seeded particle patterns is determined by cross-correlating the two images. Given the distance each group of particles moves and the time between each exposure, the two dimensional velocity vectors for each particle can be created. From these images, an average velocity map can be produced to represent the flowfield for each forcing frequency. Post processing can then be used to determine the centerline velocity with increasing downstream distance. Comparing several forcing cases can reveal which frequencies cause the velocity to decrease more rapidly. This decrease in velocity is the direct result of the existence of large-scale structures within the flow, which in turn indicates increased mixing.

The quality of PIV results is largely dependent on the quality of images acquired. There is a large amount of variability involved in the seeding of the jet flow, which makes it increasingly difficult to correlate two successive images. There also exists a significant amount of variability in the intensity of the laser sheet passed across the flow. Therefore the intensity of the light captured by the CCD camera from the seeded particles varies, leading to variations between collected images. Particles that are highly illuminated in one image may appear very dim in the next, complicating the correlation procedure. Image filtering and processing can be used to improve contrast and sharpness in images, allowing increased ease of particle detection. Cross-correlation and image processing is accomplished through the use of the PIV software package provided by

LaVision. Further post-processing of images for appropriate figures can be done using MATLAB.

### *3.4 Other Techniques*

Schlieren technique also provides a relatively quick qualitative analysis of the flow field. Schlieren technique is based on the gradients in refractive index of the flow. A light source is used in conjunction with parabolic mirrors and other optics to pass a beam of light across the flow field. The light beam is then directed onto a CCD camera that captures the images (Settles 2001). As different structures appear within the flow, the different gradients of refractive index within the structures allow them to become visible. Such a test allows undesired structures such as shock waves to become observable. The presence of either compression or expansion shock waves indicate that the jet is not at the required stagnation pressure for the corresponding design Mach number of the jet. The stagnation pressure can then be readily adjusted to reduce shock waves, thus ensuring the integrity of the experimental results.

In addition to flow visualization, PIV and schlieren, there are several other techniques utilized to record flow information. Pressure measurements provide a method of determining the preferred forcing frequency of the jet. These measurements are made by placing fast response pressure transducers within the flow near the nozzle lip. The transducers are then moved to pre-determined downstream locations to record the time trace of the pressure fluctuations within the flow. By taking the Fourier transform of the collected data, the growth, saturation and decay of the pressure fluctuations at the forcing frequency are tracked.

### *3.5 Experimental Facility*

Researchers at the GDTL have already completed a series of experiments using plasma actuators within the facility, and thus, are already equipped to handle experiments required by the present research. The complex houses a jet facility within an optically accessible anechoic chamber. This facility has removable paneling to allow for easy viewing access as well as a full set of absorptive wedges for acoustic measurements and flow diagnostics. The jets are formed using converging as well as converging-diverging nozzles for both subsonic and supersonic flows operating at various design Mach numbers. The air is conditioned in a stagnation chamber before passing through the nozzle, across the test section, and through an exhaust pipe. A schematic of the jet facility and nozzle detail can be seen in Figure 3 below.

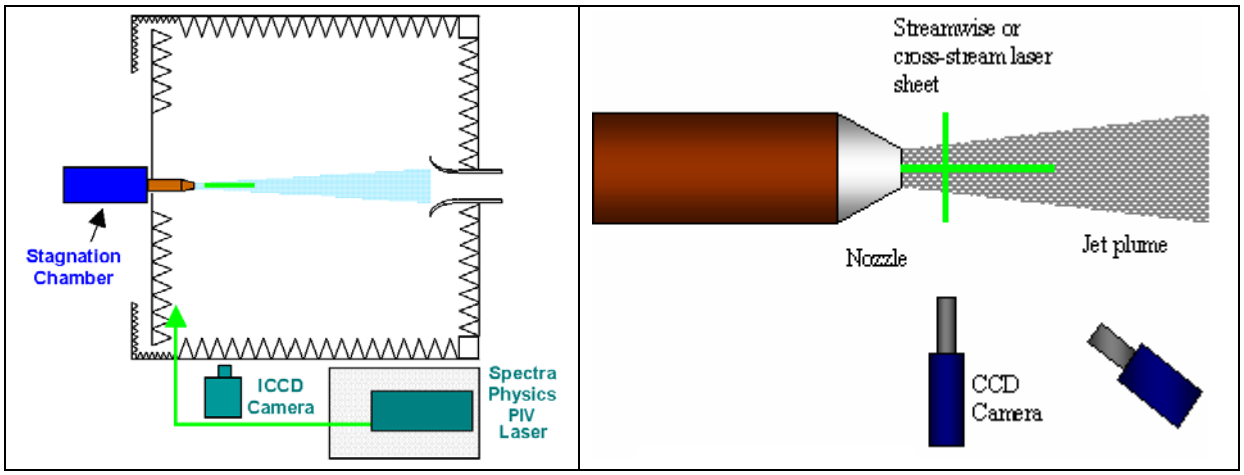


Figure 3. Jet facility schematic and nozzle detail.

Throughout testing and experimentation, both the behavior of the plasma actuators and the flow are observed. The current and voltage through the actuators are monitored and recorded using a Tektronix P6015A high voltage probe and a Tektronix AM503S wide frequency range current probe. These devices record a time history of the data being observed. There are three primary test variables involved when testing to find optimum mixing enhancement; frequency, duty cycle, and phase. Frequency, as

previously mentioned, is characterized through the use of the Strouhal number and represents the frequency of actuation. This variable is the most important factor affecting the resultant degree of mixing. Duty cycle refers to the ratio of time the actuator is "on" to the period of actuation. A lower duty cycle results in less power consumption but can lead to misfiring if not properly monitored. Duty cycle is adjusted primarily to find a balance between actuator performance and power consumed. A visual depiction of duty cycle is given in Figure 4 below.

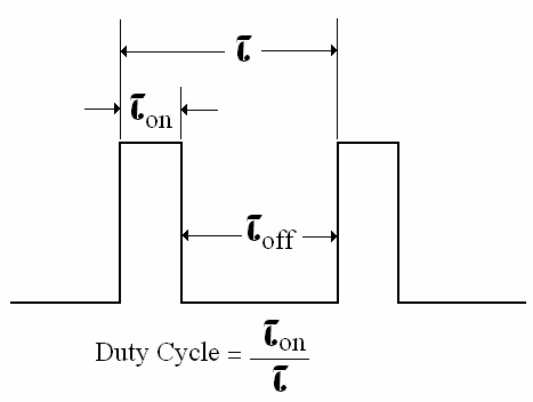


Figure 4. Definition of plasma actuator duty cycle.

Lastly, phase refers to the sequence of actuator firing. Two main modes can be excited in a rectangular jet; a symmetric mode, where all actuators fire at once, and a flapping mode where a 180° phase shift is present between the upper and lower actuators. Additional phase shifts such as 60°, 90°, etc. can be explored for purely academic reasons, but will not be considered in this study.

### *3.6 Extension Design*

For testing purposes, a nozzle extension had to be developed in order to support the electrodes used to create the plasma actuators. A digital photograph and a Solid Works 3-D drawing of the nozzle extension appears in Figure 5. This extension design

was based upon previous models to allow easy connection to the supersonic rectangular nozzles already in use at the GDTL. These nozzles have a 3:1 aspect ratio with a nozzle height of 0.5 inches, and width of 1.5 inches. Boron nitride was selected as the material for the nozzle extension based upon the success in its use in similar projects (Samimy et. al. 2004, 2007a & 2007b). Boron nitride has excellent thermal properties and thus is able to withstand the harsh environment imposed by the generation of plasma. This material is however, very soft, porous, and susceptible to wear. For these reasons, several precautions had to be taken in the design of a suitable nozzle extension. The most critical element of the design is the placement or orientation of electrodes. Due to the high voltages being sent through the electrodes, they must either be completely insulated or else positioned such that the closest distance between them becomes the tip of the electrode where arcing is desired. The porosity of the material necessitates that the electrodes be far enough away from each other within the extension to prevent internal arcing. To accomplish this task and yet still keep electrodes at the required 3.5 mm spacing, individual electrodes were given offset angles of 10° and 16°. The angle also ensured that there would be enough material between the exterior of the extension and the electrode to give the piece sufficient strength and not fail throughout machining or ensuing testing. To produce the desired effect, actuators must be placed as close to the trailing edge of the nozzle extension as possible. These angles allowed electrodes to be positioned correctly in the flow while maintaining acceptable clearances. A groove was also introduced into the design to allow the electrodes to sit in. Previous experience has shown that without such considerations, plasma may not remain stable and may be blown downstream under high-speed flows. This groove provides a sufficient barrier to make

sure no such incident occurs. Plastic screws for securing electrodes were also incorporated into the design to prevent abrasive contact with metal components that may damage the delicate material. The extension itself can be attached to the nozzle without the use of threaded fasteners. Therefore, metal screws were utilized to attach the extension to the nozzle surface. This freedom permitted minute alignments to be made to make certain the nozzle was placed in the correct position.

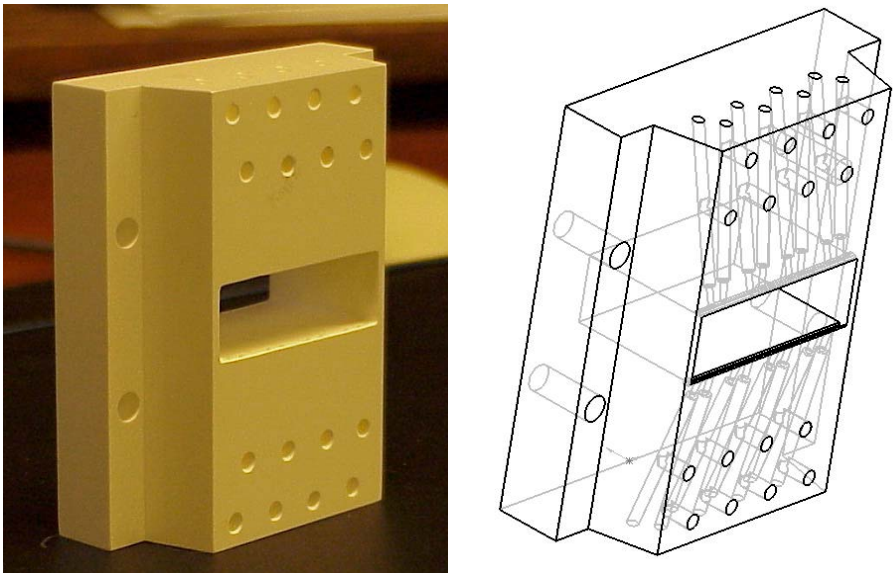

Figure 5. Rectangular boron nitride nozzle extension.

The electrodes used in all experiments were made of tungsten. This material was also used successfully in previous endeavors. In order to prevent arcing outside of the extension, paper is used as an insulator by rolling a small strip and wrapping it around the electrode before placing into the corresponding hole. Common car retouching paint has also been used to coat the electrodes and add an additional layer of protection. Under some circumstances, such as when running with a Mach 2.0 nozzle, the exiting air becomes rather cold. This in turn cools the extension, causing condensation to form on its surface. Paper alone is not enough to prevent arcing in this situation since it absorbs

water and becomes very wet itself. Paint can, in most circumstances, add enough additional insulation to prevent arcing even as this condensation forms. The following Figure 6 shows the extension and electrode connection once the extension is implemented for testing.

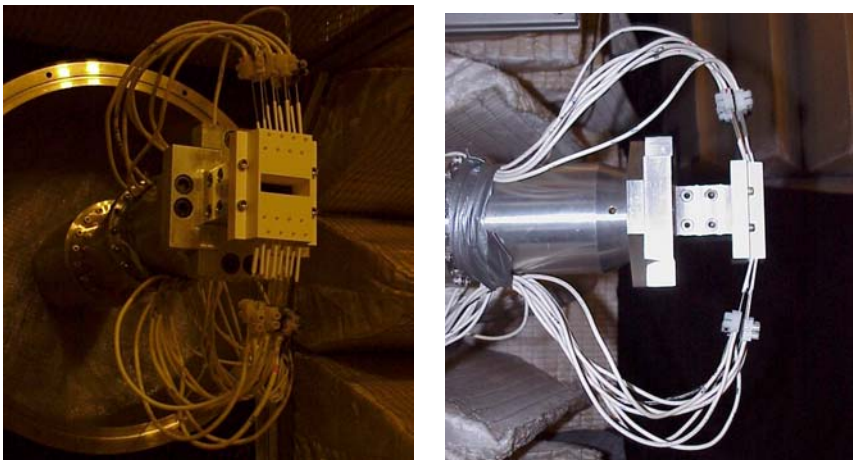

Figure 6. Ceramic extension and electrode experimental setup.

# 4. Preliminary Results

## *4.1 Initial PIV Attempts*

The first set of tests that were conducted was particle image velocimetry tests. There was a small window of time available for some possible testing near the end of the quarter, and with PIV equipment already present within the lab, an attempt was made at obtaining some quality PIV results. The tests were performed on a Mach 1.3 jet in the flapping ($m = \pm 1$) mode. Eight actuators were used, four evenly spaced on the top and bottom of the extension with approximately 6.5 mm spacing and 3 mm spacing between electrodes. The intent of the experiment was to show that the extension could operate under all required conditions and that plasma actuation could increase the degree of mixing present in the jet under various forcing frequencies. A theoretical preferred frequency was calculated as previously shown based on a Strouhal number of 0.25 to be roughly 9900 Hz. A range of frequencies was tested surrounding this frequency to increase the likelihood that the actual preferred frequency could be found. The PIV testing process produces pairs of images that are subsequently processed to produce average velocity maps for each forcing frequency. The following figure displays the results for both the baseline case and the frequency for which the maximum amount of mixing was observed.

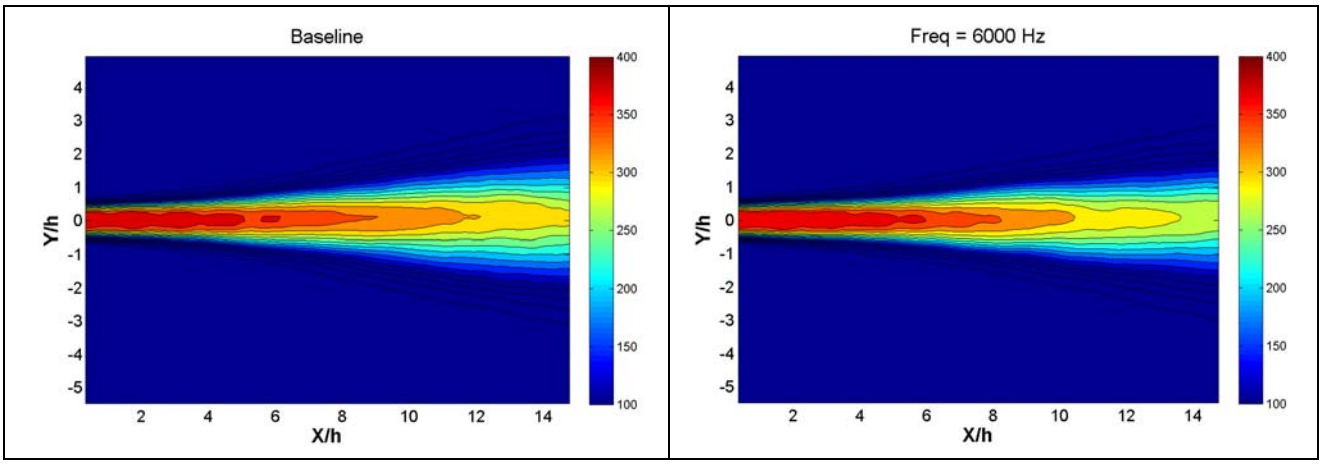


Figure 7. Velocity contour plot with downstream distance for varying frequency.

As Figure 7 above shows, there is definite variation in the velocity profile of the jet under each of the forcing cases. The 6 kHz case was found to alter the velocity field the most of all the frequencies tested. This result was not initially predicted, but an observation made during testing confirmed that proper testing conditions were not upheld throughout the entire testing sequence. It was observed that arcing of the plasma occurred outside of extension that may have led to slightly unexpected results in other forcing cases. The preferred frequency of the rectangular nozzle was calculated to be around 9-10 kHz. The figure shows the core of the jet to be slightly shorter in the 6 kHz case, showing that there was indeed more mixing around this forcing frequency. The presence of shock cells can also be seen in the wavy pattern of the jet core, which may have contributed to the slightly skewed results. The following figure shows the resultant variations in centerline velocity measured for each forcing frequency.

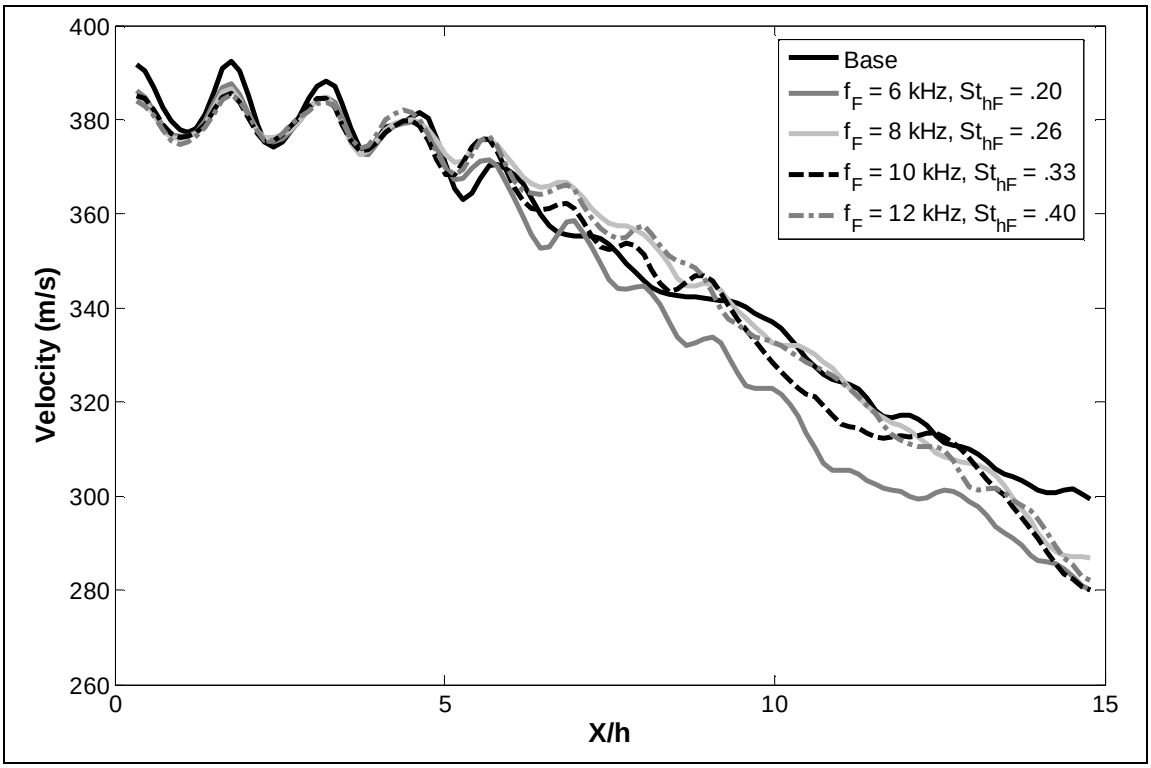

Figure 8. Centerline velocity with downstream distance for varying frequency.

Figure 8 shows the fluctuations in centerline velocity as the flow moves downstream for each forcing frequency. As expected, the baseline case is not slowed down as much as the forcing cases, suggesting the presence of structures (and thus mixing) produced within the flow under forcing. It can also be seen that at 6 kHz, the flow is reduced the greatest amount, possibly confirming the existence of the first jet instability to be around this frequency.

As previously mentioned, there were some difficulties throughout testing that may have made direct interpretation of results difficult. After the first few forcing cases, it was noticed that there was some arcing between electrodes outside of the extension. It is unclear when this arcing began and during which forcing frequency. Being the first case tested, 6 kHz may represent the best data collected throughout the experiment.

Regardless, it is clear that this forcing frequency resulted in an increased degree of mixing over other frequencies.

As a result, to prevent such arcing in future testing, the electrodes were painted to add an additional layer of insulation. With the electrodes properly insulated, further work using PIV and flow visualization were used to verify the possible existence of a preferred frequency in the 6-8 kHz range. Although this battery of tests was not ideal, the PIV results confirmed that the extension could be used to collect such results. The data processing procedure also provided insight into data reduction and presentation techniques that could be applied to subsequent data sets.

### *4.2 Initial Flow Visualization Attempts*

The first series of tests conducted using the rectangular nozzle were flow visualization experiments performed in late October. Due to the lack of high temperatures and humidity, a Mach 2.0 jet was used rather than a Mach 1.3 jet, as was originally planned. The room temperature was 22°C at the start of testing, with an initial humidity of 39%. This humidity represented the higher end of the limit of acceptable humidity levels, but weather forecasts showed significantly lower temperatures in subsequent days. Therefore, the experiments were run despite not having ideal humidity levels. As previously mentioned, flow visualization depends on the condensation within the shear layer and the capturing laser light scattered from these particles. A Princeton Instruments Pixis 400 camera with a Nikon Zoom Nikkor 70-300mm lens was used to capture these images. A schematic of the experimental setup can be seen in Figure 3 above. These images were then transferred to a computer through a USB cable. Each file recorded contained 71 images. A snapshot of a dot card was also taken in order to

convert distance in pixels to a physical distance in inches. Using this dot card image, the number of pixels between each successive pair of dots was recorded and then averaged. With the known dot spacing of 20 mm, a conversion factor could be established. For this experiment, this value was calculated to be 0.23613 mm/pixel. This value also allowed the nozzle height to be converted to pixels. A height of 0.0127 m (0.5 inches) was found to be 53.78 pixels. Knowing this quantity allowed the tick marks seen within the subsequent figures to be placed at integer values of jet nozzle height downstream.

As previously stated, the preferred frequency of a Mach 2.0 nozzle with height 0.0127 m (0.5 inches) and tank stagnation temperature of 10°C was found to be approximately 9900 Hz. The rectangular nozzle extension was again designed to house eight actuators, equally spaced at 6.5 mm along the top and bottom of the nozzle exit with 3 mm spacing between electrodes. All tests were preformed in the flapping mode with the top and bottom actuators exactly 180° out of phase. The following table summarizes the experimental scenarios recorded.

Table 1. Initial flow visualization test matrix.

| $St_{hF}$ | 0.051 | 0.101 | 0.152 | 0.202 | 0.227 | 0.253 | 0.278 | 0.303 | 0.354 | 0.404 | 0.505 |
|---|---|---|---|---|---|---|---|---|---|---|---|
| $F_F$ (kHz) | 2 | 4 | 6 | 8 | 9 | 10 | 11 | 12 | 14 | 16 | 20 |
| DC (%) | 5 | 5 | 5 | 5 | 5 | 5 | 7 | 7 | 7 | 7 | 7 |

As this table shows, the number of frequencies surrounding the estimated 9900 Hz preferred frequency was increased to discern whether or not the theoretical preferred frequency was representative of the experimentally determined value. Figure 9 below displays the average flow visualization images for the baseline and two selected frequencies; 6 and 10 kHz. The 6 kHz case was chosen due to the fact that the effect of forcing can be clearly seen. The 10 kHz case was chosen not only because of its close

proximity to the theoretically calculated preferred frequency, but also because the observed response of the flow was representative of the majority of other cases.

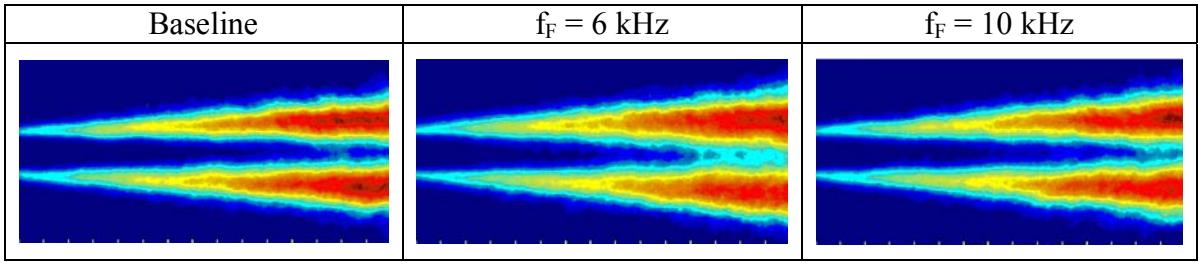


Figure 9. Average flow visualization images for Mach 2.0 nozzle. Images begin approximately 110 mm from nozzle exit; tick marks have 12.7 mm spacing.

As the images show, the effect of forcing does have visible effects on the length of the potential core. Under 6 kHz forcing, the core was appreciably reduced. For several other forcing frequencies the core was noticeably shorter than the baseline case, but was not significantly reduced. Mixing in the first few nozzle heights downstream may also have been increased, but are not displayed in the above figure. In order to record more flow information farther downstream, the images presented here start at a distance of 3 jet heights downstream of the nozzle exit. Further investigation into the effect of forcing on the width of the shear layer may be needed to show relative amounts of mixing between theses cases.

Figure 10 contains instantaneous flow visualization images for the three cases presented above. The following images were selected due to the fact that they represent the "best" cases observed for each forcing case. It should be noted, however, that images exist in both 6 and 10 kHz cases that closely resemble the baseline images.

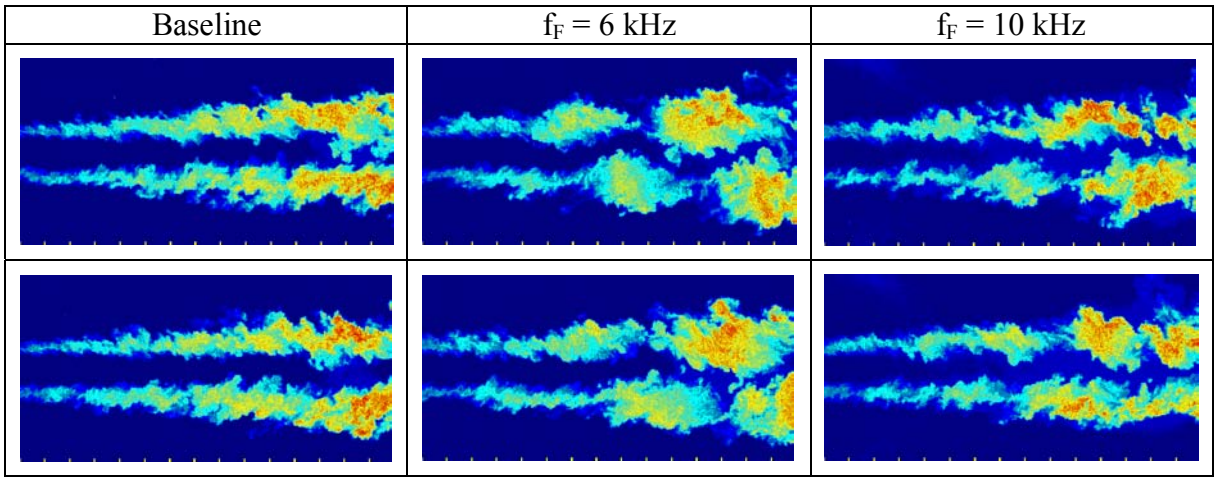

Figure 10. Instantaneous flow visualization images.

As can be seen in these figures, the 6 kHz forcing frequency appears to stimulate the development of large structures within the flow that form a clear flapping pattern. Similar patterns exist in the 10 kHz case, but are not as obvious. The structures are also not as clearly defined.

There may be several other factors affecting the development of structures within these flows. Most importantly, the nozzle was not operated at the exact required stagnation pressure for the design Mach number. This may have caused shock cells to form within the flowfield. The structures observed at the 6 kHz forcing case might be the combined results of these shock cells and the effect of control. Had the flow been ideally expanded not only would the structures have been more readily observed, but the flow may also have been more responsive to control.

### *4.3 Flow Visualization Investigation and Improvement*

#### 4.3.1 Introduction

As previously mentioned, further testing was required to provide a more accurate assessment of the effect of control on a Mach 2.0 rectangular jet. The required stagnation pressure must be calculated in order to keep the flow as uniform as possible to avoid

interference from shock cells. Phase locking may also be explored to reinforce the development of large structures under given forcing frequencies. In addition, images could then be phase-averaged and compared with instantaneous images to either prove or refute the effect and degree of control authority imposed by specified forcing frequencies. Two aspects of the flowfield were initially investigated; duty cycle and stagnation pressure.

### 4.3.2 Duty Cycle Study

Initial flow visualization testing showed the need for further investigation into the behavior of the plasma and possibly the required stagnation pressure. In order to observe plasma behavior, a current trace was taken for two actuators to determine if they were firing properly with the experimental duty cycle used throughout testing. For the first round of testing, two actuators were selected for experimentation; one actuator from each the top and bottom and on opposite side of the nozzle. It was observed that one of the actuators (actuator 3 in Figure 11) was not firing properly for the given 8 kHz input signal under a variety of scenarios. The last attempt made to determine the cause of this behavior involved adjusting the duty cycle of the actuator pulse. The figure below shows the resultant current probe traces for the misfiring actuator and the actuator behaving properly.

In order to determine what may have caused the formation of structures within the baseline flow case, several tests were performed to both study actuator behavior and determine the true stagnation pressure for the design Mach number. In order to observe actuator behavior, a current and voltage trace was recorded over 30 cycles of actuator firing. A LeCroy oscilloscope was used to record these traces. If several anomalies or

other misfires are observed throughout the trace, actuator firing may be the main issue to consider when performing flow visualization again. Current traces were recorded for frequencies of 4, 6, 8, 10, 12, 16, 20, and 30 kHz. Two sets of electrodes were selected in order to observe actuator behavior. As previously mentioned, the two actuators selected were positioned on opposite sides of the nozzle. The following Figure 11 contains the resultant current traces. The dark jagged waveform represents the actuator current, whereas the faint square waveform represents the input pulse. Analysis of the current traces showed that although one actuator was firing regularly, the other only fired consistently for a few of the selected frequencies and exhibited irregular behavior for most of the others. To better understand the issue, further tests were run while firing a single actuator at a time to allow easier visual observation of the actuator within the chamber. Several cases were tested with no real detectable results. One actuator appeared to be firing, but at decreased amplitude when compared to other actuators. The final scenario involved testing the problematic actuator under 5% and 20% duty cycle at 8 kHz. The 5% case still showed improper firing, but for 20% duty cycle, the actuator appeared to operate properly. The results can be seen in the following figure.

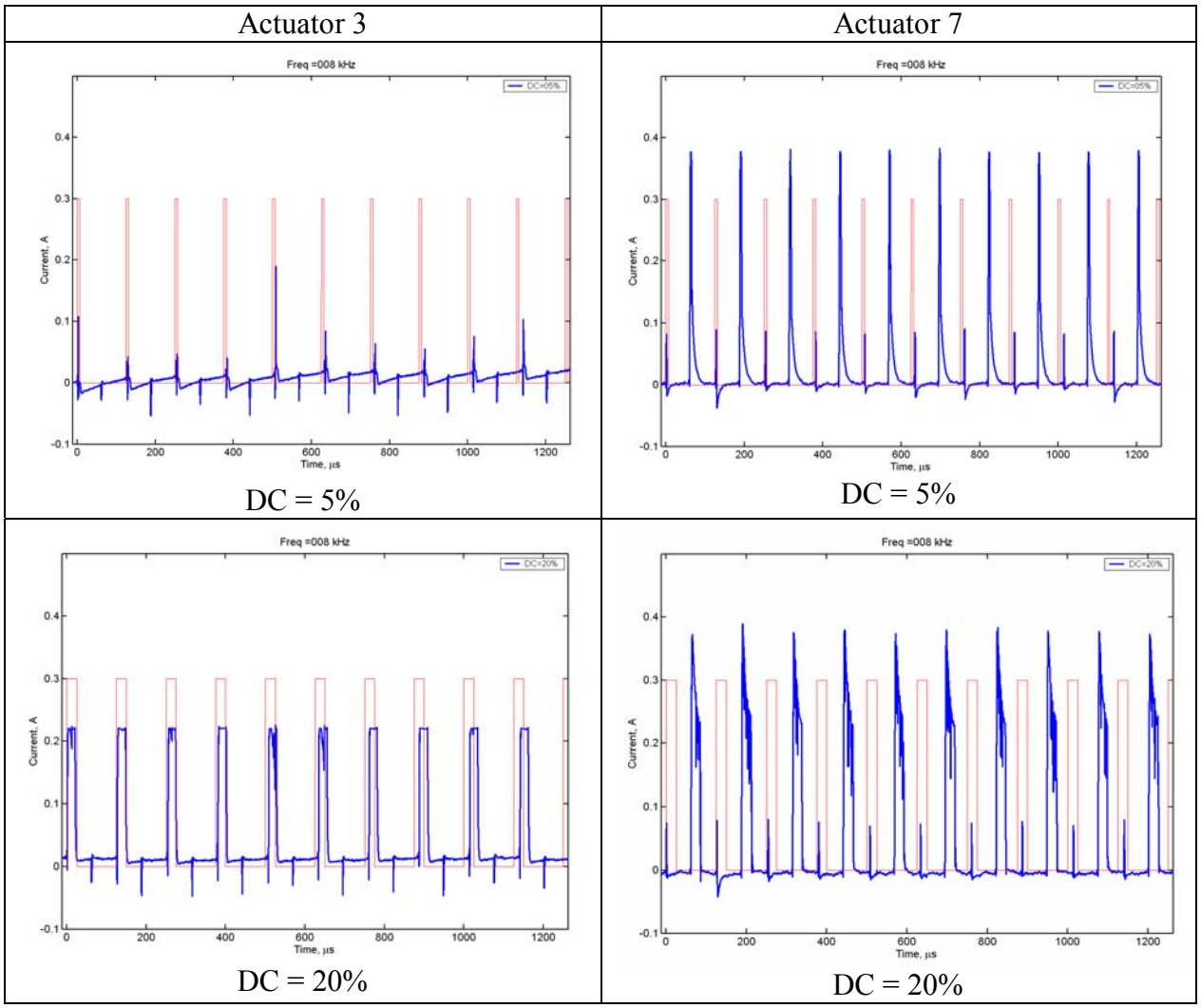


Figure 11. Effect of duty cycle on actuator behavior under 8 kHz forcing.

As this figure shows, for an 8 kHz input signal, adjusting the duty cycle significantly affects the actuator's ability to arc and sustain the plasma. For an 8 kHz signal with a 5% duty cycle, the actual pulse duration becomes 6.25 µsec. Once increased to 20% duty cycle, the pulse duration is increased to 25 µsec. This increase in pulse duration allows the actuator ample time to sustain an arc and therefore have an effect on the system. This phenomenon was explored further in an additional round of tests, this time looking at the effect of changing pulse duration rather than duty cycle.

Rather than simply setting duty cycle, pulse durations of 20, 15, 10 and 5 μsec were chosen instead. The duty cycle was then calculated using the following equations.

(6) $$\tau = \frac{1}{f_F}$$

(7) $$\tau_{PL} = \delta * \tau$$

where τ is the period of the input signal, δ is the duty cycle, and $\tau_{PL}$ is the pulse duration. For this round of testing, two arbitrary actuators were again chosen due to the fact that they were positioned on opposite sides of the nozzle and were located near the centerline of the flow. It may have been favorable to use the same actuators as were used in the initial round of testing, but due to a reconfiguration of the system between test dates, such consistency was not possible. It is important to note that there is also inconsistency regarding the amplitude of the current traces between the following actuators. The physical condition of the actuator (such as cleanliness, for example) can affect the magnitude of the output waveform. Therefore, the magnitude of the observed current trace is much less important than the actual event of actuator firing. The following figure displays the results for the 10 kHz case for the previously stated pulse durations.

| Actuator 2 | Actuator 6 |
|---|---|
| 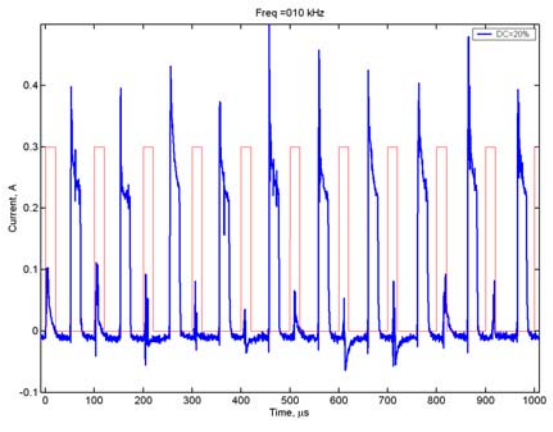 | 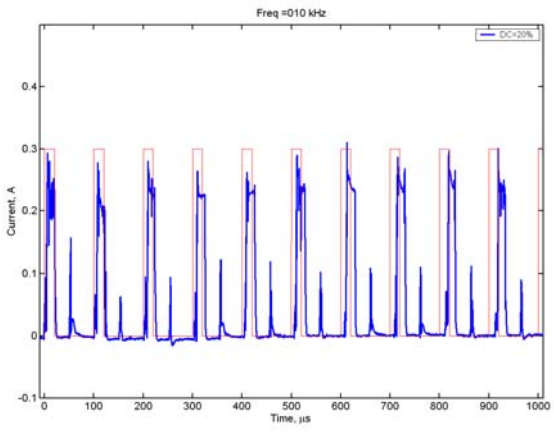 |
| $\tau_{PL}$ = 20 μsec, DC = 20% | $\tau_{PL}$ = 20 μsec, DC = 20% |

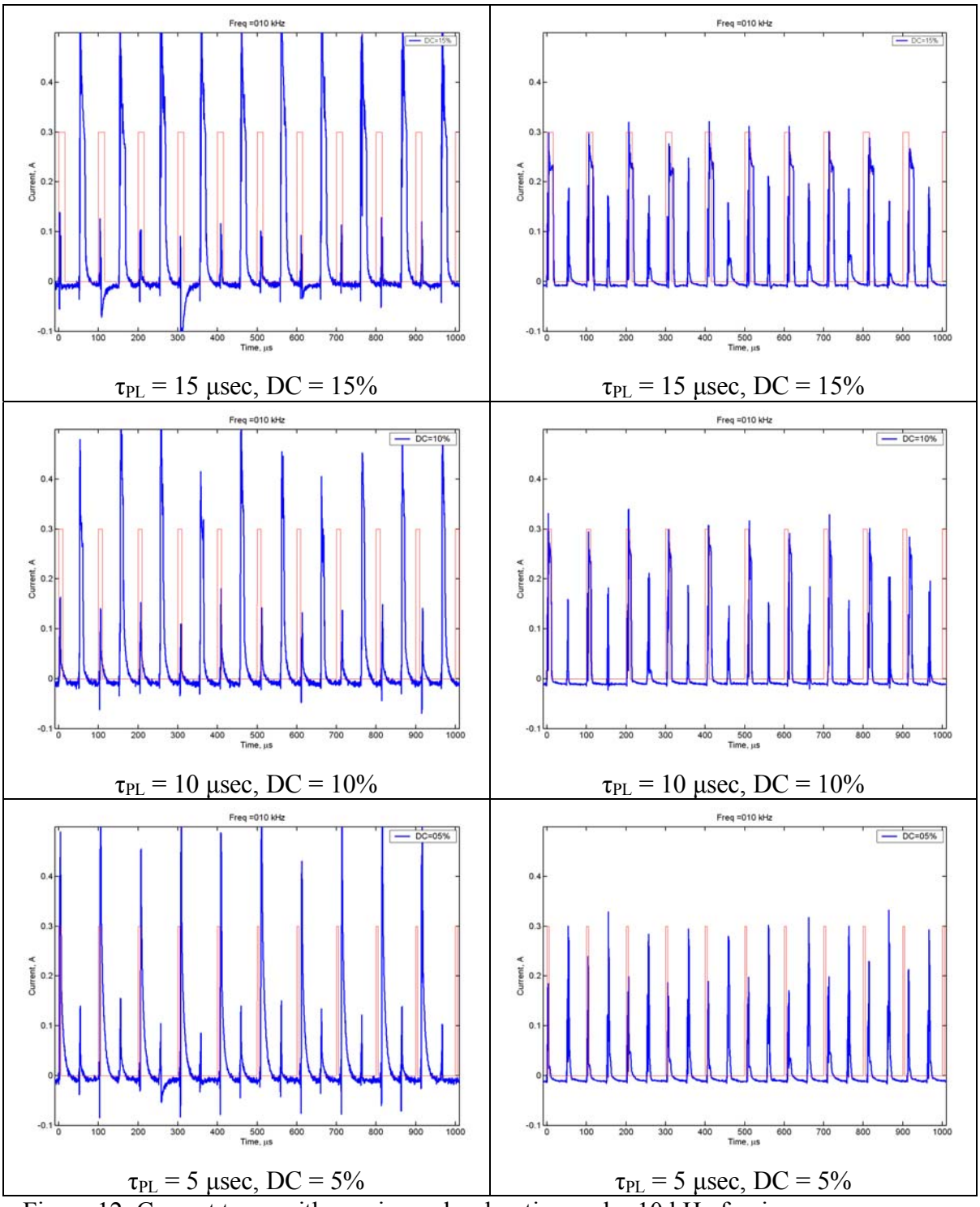


$\tau_{PL}$ = 15 µsec, DC = 15%

$\tau_{PL}$ = 15 µsec, DC = 15%

$\tau_{PL}$ = 10 µsec, DC = 10%

$\tau_{PL}$ = 10 µsec, DC = 10%

$\tau_{PL}$ = 5 µsec, DC = 5%

$\tau_{PL}$ = 5 µsec, DC = 5%

Figure 12. Current trace with varying pulse duration under 10 kHz forcing.

As the figure above shows, both actuators fired properly over all pulse durations tested. This is somewhat inconsistent with previous results, but may be attributed to the quality of the actuators being used throughout each test. Between test dates some

electrodes were broken and needed replaced, while still others were cleaned to improve efficiency. What is important to observe from these results is that the actuator current trace becomes more like a spike at smaller duty cycles. This short duration may still show that the actuator is firing, but may not be properly setting up the required arc. The actuator current steadily decreases in magnitude as the frequency and thus duty cycle are increased, but this is due primarily to the rather large duty cycles required at higher frequencies. In addition, for the 20 kHz case and above, the duty cycle is nearly half the period of actuation. Such a large duty cycle may not be allowing the actuator ample time to cool between firings. If the electrodes are not sufficiently cooled, the actuator remains at a high temperature and the required pulsing effect of the actuator diminishes. Typically for testing at GDTL, duty cycles larger than 30% are rarely ever used. Due to the sharp current traces observed at lower pulse durations, a pulse duration of at least 10 μsec was recommended for subsequent flow visualization testing.

### 4.3.3 Stagnation Pressure Investigation

In order to determine the required stagnation pressure to produce a uniform flow field at the specified design Mach number, acoustic measurements were made. A ¼" Bruel & Kjaer microphone (Bruel & Kjaer Model 4939) was placed at a location 90° to the nozzle exit. The nozzle was also rotated to ensure the flapping mode of the jet could be accurately measured. Tests were conducted with stagnation pressure of 84 psig, and in 2 psig increments starting at 88 psig up to 110 psig. The ambient pressure on test day was 14.01 psia. Each block of data included 8192 points at a sampling rate of 200 kHz, and a total of 50 blocks were taken. Once recorded, the data was imported into MATLAB in order to separate the blocks of data and perform FFT analysis on these data

sets to show the spectrum for each stagnation pressure. The spectral shape is directly correlated to the type of flow regime established at the nozzle exit. As the following plots show, it is clearly visible from the acoustic data whether the jet is under- or over-expanded. For over-expanded flows, strong tonal peaks can be seen at the natural frequencies of the jet. The flow then passes through a transition in which the peaks flatten out, representing the ideally expanded condition, or the condition in which exit pressure equals the ambient pressure. Moving further into the under-expanded flow regime, the peaks begin to reappear. The primary difference can be seen, however, in the second peak. Rather than being sharp and distinct as in the over-expanded case, the peak begins to widen as the jet becomes under-expanded. From the following plots, it can be seen that the ideal stagnation pressure for the Mach 2.0 jet can be found in the vicinity of 92 psig. Moving the stagnation pressure in either direction results in the formation of sharp increases in sound pressure level as the natural frequencies of the jet again become more visible. For the given 14.01 psia pressure on test day and the experimental stagnation pressure of 92 psig, the following equation can be used to determine the actual Mach number of the nozzle (Anderson 2004).

$$\frac{P_o}{P} = \left(1 + \frac{\gamma - 1}{2} M^2\right)^{\frac{\gamma}{\gamma - 1}} \tag{8}$$

This value was cal culated to be 1.978, showing that the nozzle being used may not guarantee an exact Mach 2.0 flow.

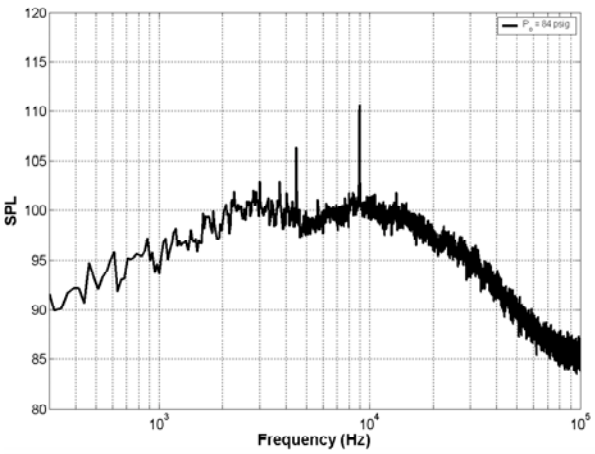


Over-expanded Condition (84 psig)

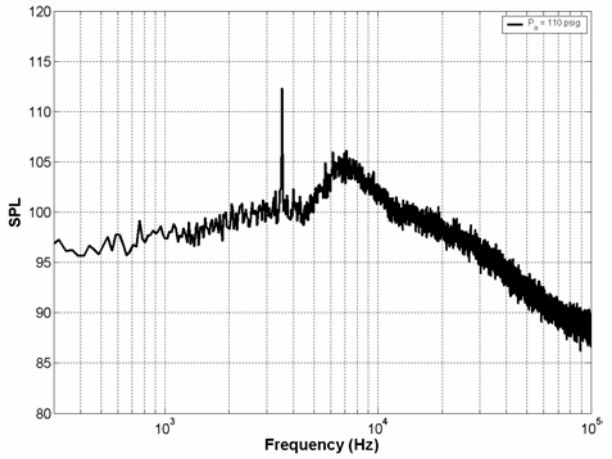


Under-expanded Condition (110 psig)

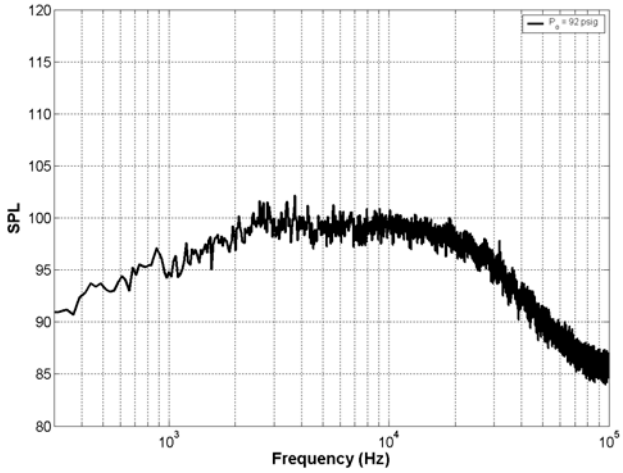


Nearly uniform flow (92 psig)

Figure 13. Comparison of SPL data with varying flow regimes.

Therefore, for subsequent testing, it was determined that the stagnation pressure should be set to a level of approximately 92 psig in order to produce as close to uniform flow as possible.

# 5. Results

## *5.1 Introduction*

The initial investigation of flow visualization showed there were several aspects of the test not fully investigated prior to data collection. This lead to a lack of confidence in the results. As the previous sections detailed, both duty cycle and stagnation pressure were investigated in an attempt to improve results. The initial data set was then both repeated and expanded for additional data collection. Based upon both the duty cycle and stagnation pressure studies, the duty cycle was primarily fixed at 10 μsec, while stagnation pressure was set to 92 psig. The following sections detailed the results of the improved flow visualization tests.

## *5.2 Flow Visualization*

After investigating methods for improving flow visualization data sets, the initial data set was again tested for hopefully improved results. As before, in order to see desired results, a Mach 2.0 jet was used rather than a Mach 1.3 jet. The room temperature was 21.5°C at the start of testing, with an initial humidity level of 31%. This humidity represented the lower end of the limit of acceptable humidity levels, but was acceptable given the late December test date and increasingly rainy days forecasted through the holiday. As before, a Princeton Instruments Pixis 400 camera with a Nikon Zoom Nikkor 70-300mm lens was used to capture these images. The experimental setup was consistent with the setup used in earlier testing. Again, each file recorded contained 71 images, and a dot card was used to convert distance in pixels to a physical distance in inches. With the known dot spacing of 20 mm, a conversion factor of 0.23613 mm/pixel was calculated. This value also allowed the nozzle height to be converted to pixels. A

height of 12.7 mm (0.5 inches) was found to be 49.068 pixels. Knowing this quantity allowed the tick marks seen within the subsequent figure to be placed at integer values of jet nozzle height downstream. As previously calculated, the preferred forcing frequency of the 0.5 inch rectangular jet at Mach 2.0 flow was calculated to be approximately 9900 Hz. As before, eight actuators were used, all equally spaced at 6.5 mm along the top and bottom of the nozzle exit with 3 mm spacing between electrodes. As an extension of the previous set of tests, both the m = ±1 (flapping mode with actuators 180˚ out of phase) and m = 0 (all actuators in phase) modes were investigation over frequencies of 4, 6, 8, 9, 10, 11, 12, 14, 16, 20, and 40 kHz ($St_D$ = 0.10, 0.15, 0.20, 0.23, 0.2526, 0.28, 0.30, 0.35, 0.4042, 0.51 and 1.01 respectively). The duty cycle was adjusted in order to preserve the aforementioned 10 μsec pulse duration. The effect of duty cycle was recorded for 4, 8, 16, 32, and 50% duty cycles while forcing at 8 kHz with the flapping mode. The following figure summarizes the experimental scenarios recorded for the averaged images. Initially following the nozzle exit, the structures generated are still small and beginning to grow through the entrainment of ambient air. At these small distances there is little time to allow sufficient growth and a lack of sufficient particles entrained, preventing these structures from being visualized. Due to this lack of visible structures directly following the nozzle exit, the camera was aimed further downstream to allow more of the desired flow behavior to be recorded. The left edge of the following images is positioned approximately 1.822 inches or 3.644 jet heights downstream of the nozzle exit.

| m = 0 | m = ± 1 |
| --- | --- |
| 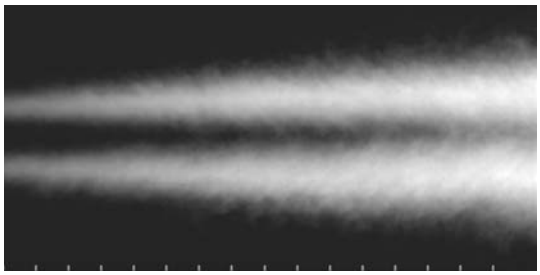 $f_F$ = 4 kHz, DC = 4% | 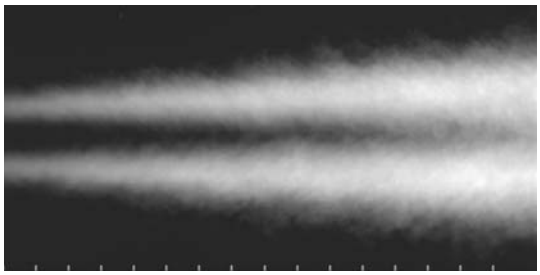 $f_F$ = 4 kHz, DC = 4% |
| 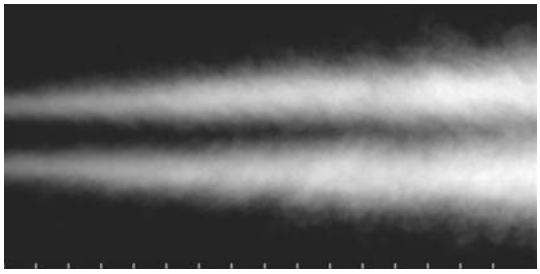 $f_F$ = 6 kHz, DC = 6% | 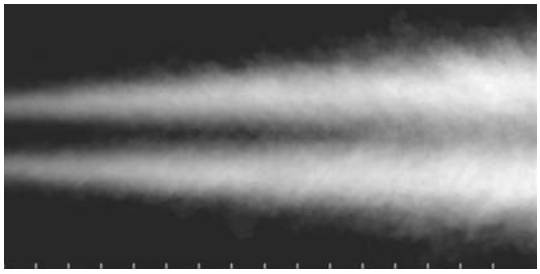 $f_F$ = 6 kHz, DC = 6% |
| 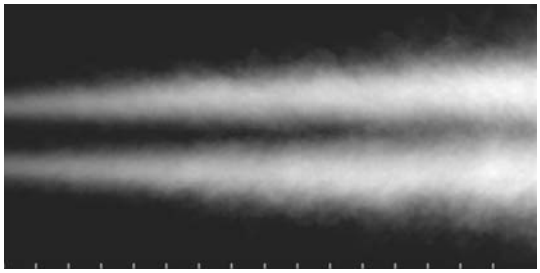 $f_F$ = 8 kHz, DC = 8% | 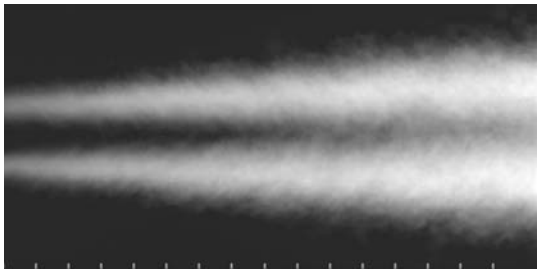 $f_F$ = 8 kHz, DC = 8% |
| 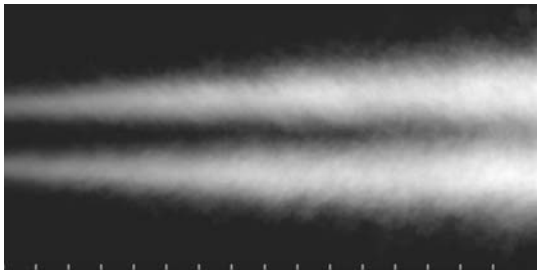 $f_F$ = 9 kHz, DC = 9% | 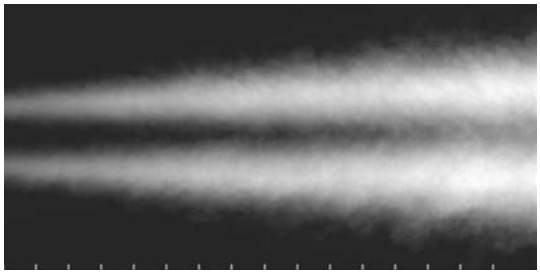 $f_F$ = 9 kHz, DC = 9% |
| 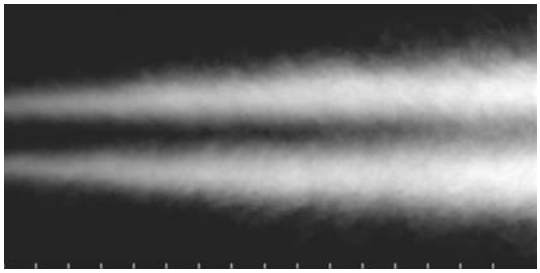 $f_F$ = 10 kHz, DC = 10% | 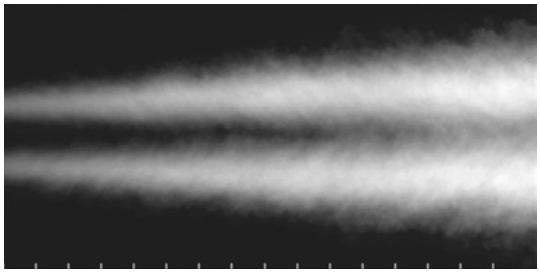 $f_F$ = 10 kHz, DC = 10% |

| | |
|---|---|
| 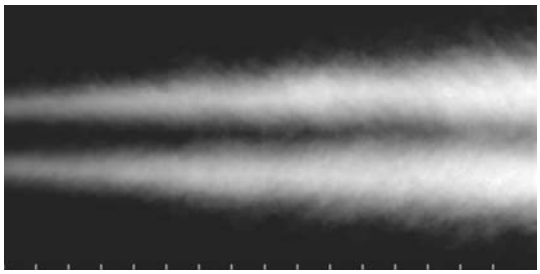 $f_F$ = 11 kHz, DC = 11% | 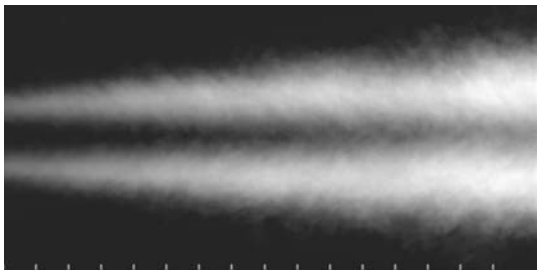 $f_F$ = 11 kHz, DC = 11% |
| 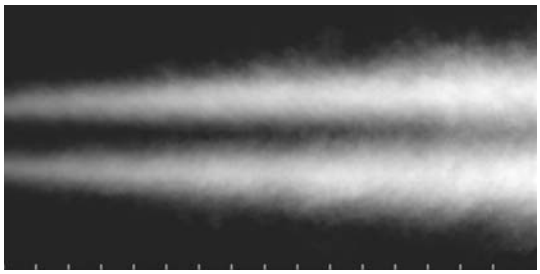 $f_F$ = 12 kHz, DC = 12% | 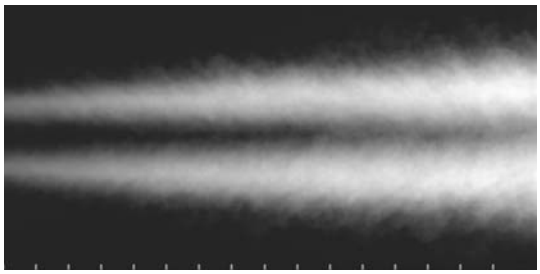 $f_F$ = 12 kHz, DC = 12% |
| 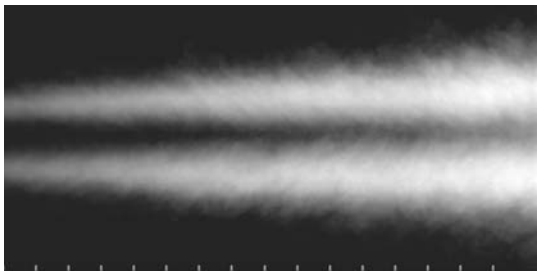 $f_F$ = 14 kHz, DC = 14% | 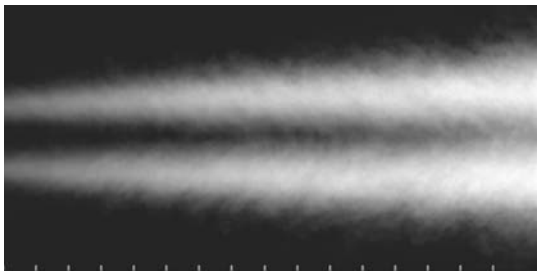 $f_F$ = 14 kHz, DC = 14% |
| 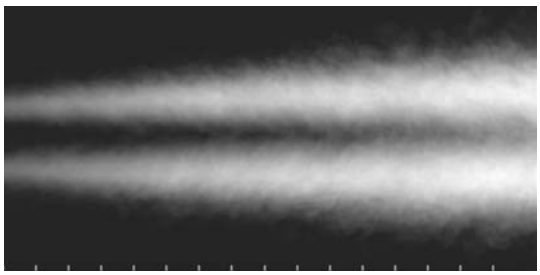 $f_F$ = 16 kHz, DC = 16% | 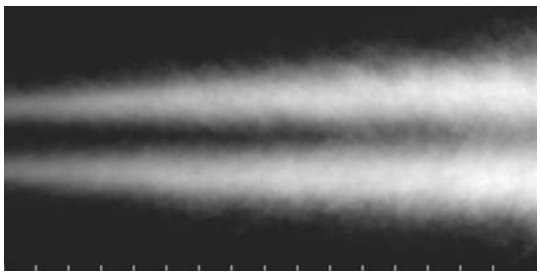 $f_F$ = 16 kHz, DC = 16% |
| 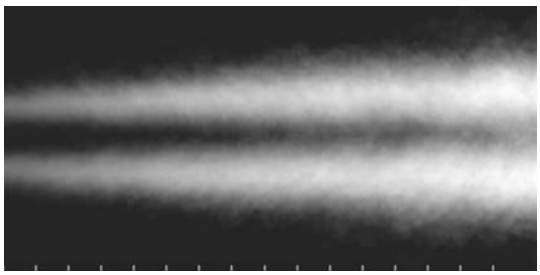 $f_F$ = 20 kHz, DC = 20% | 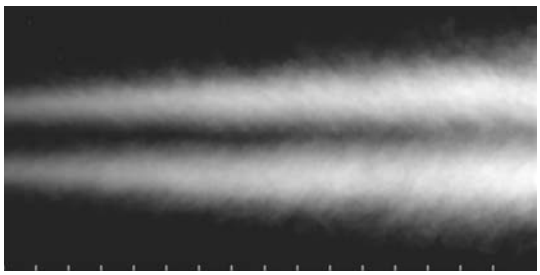 $f_F$ = 20 kHz, DC = 20% |

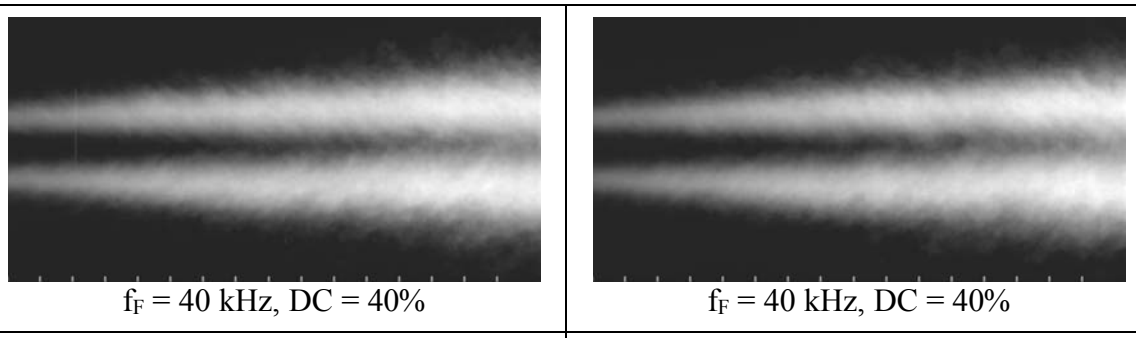

$f_F$ = 40 kHz, DC = 40%



$f_F$ = 40 kHz, DC = 40%

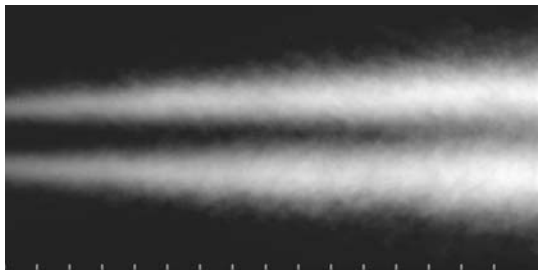

Baseline

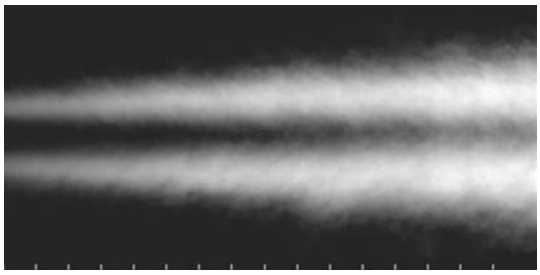

Baseline

Figure 14. Average flow visualization images.

As the above images show, in most instances the flapping mode outperforms the in-phase mode, which is as expected. The flapping mode creates larger structures that entrain larger amounts of ambient air into the flow, increasing mixing and therefore shortening the potential core of the jet. The most significant reductions can be seen in the 6-8 kHz range, suggesting that the preferred frequency of the flow is somewhat lower than the predicted 9900 Hz. It can also be seen that the length of the potential core becomes roughly 12.5 jet heights downstream of the flow in the most optimum cases, reduced from approximately 15.5 jet heights for the baseline case. The initial prediction of preferred forcing frequency was based on a Strouhal number of 0.25, whereas the preferred frequency range described above corresponds to Strouhal numbers from 0.15 to 0.20. It should be noted that the assumed Strouhal number of 0.25 was one of several estimates found throughout an extensive literature review. The literature shows significant variations in Strouhal number ranging from roughly 0.10 to as high as 0.6, placing the experimental result well within the expected range. This range of Strouhal

numbers does however also lie within results from other previous work conducted at GDTL, as will be shown in subsequent discussion (Kerechanin 2000).

| m = 0 | m = ± 1 |
|---|---|
| 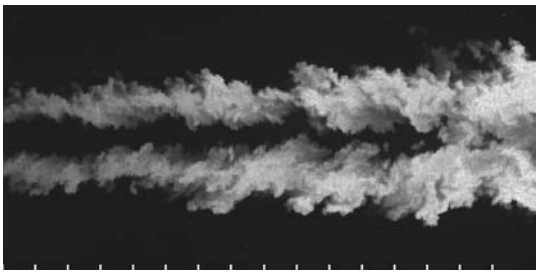 $f_F$ = 4 kHz, DC = 4% | 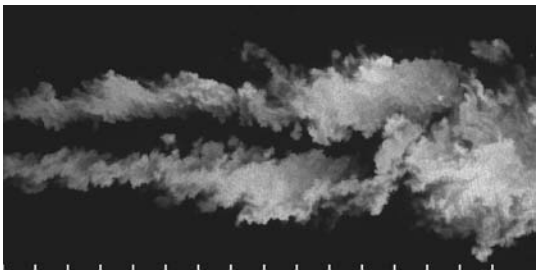 $f_F$ = 4 kHz, DC = 4% |
| 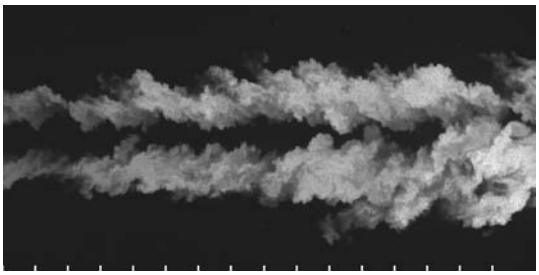 $f_F$ = 6 kHz, DC = 6% | 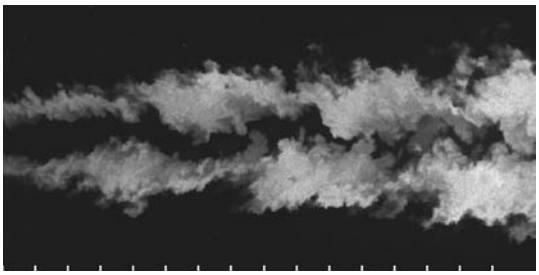 $f_F$ = 6 kHz, DC = 6% |
| 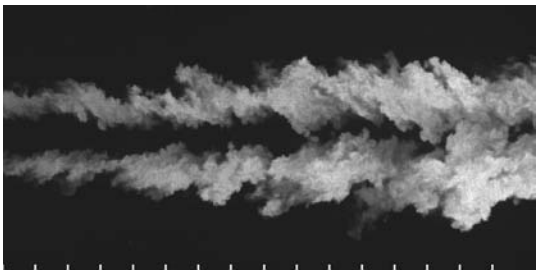 $f_F$ = 8 kHz, DC = 8% | 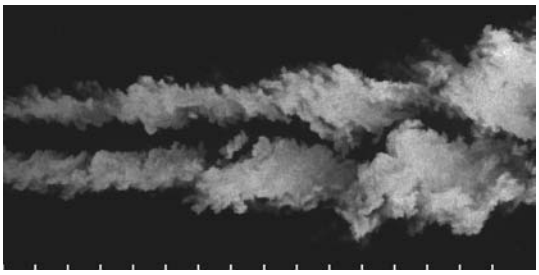 $f_F$ = 8 kHz, DC = 8% |
| 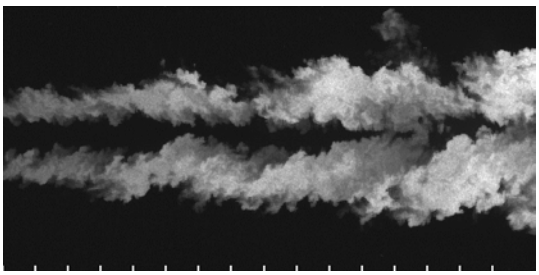 $f_F$ = 9 kHz, DC = 9% | 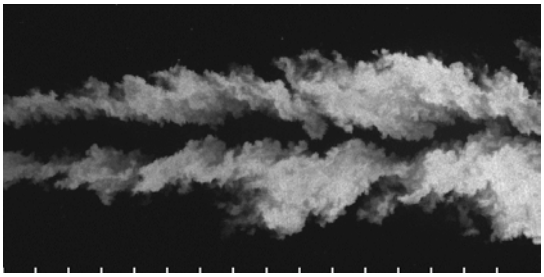 $f_F$ = 9 kHz, DC = 9% |

| | |
|---|---|
| 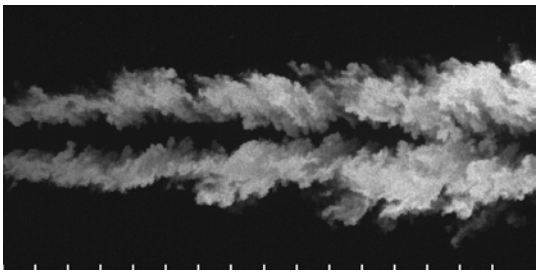 $f_F$ = 10 kHz, DC = 10% | 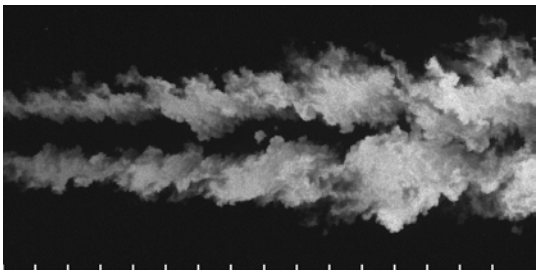 $f_F$ = 10 kHz, DC = 10% |
| 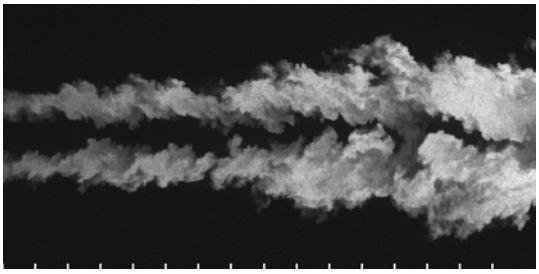 $f_F$ = 11 kHz, DC = 11% | 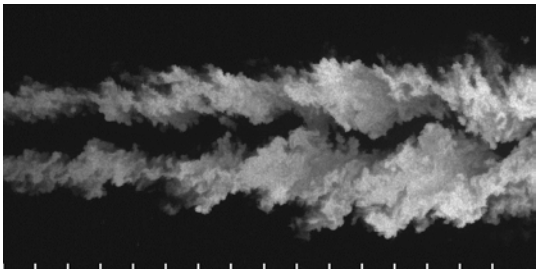 $f_F$ = 11 kHz, DC = 11% |
| 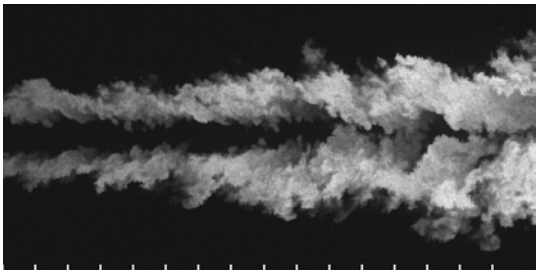 $f_F$ = 12 kHz, DC = 12% | 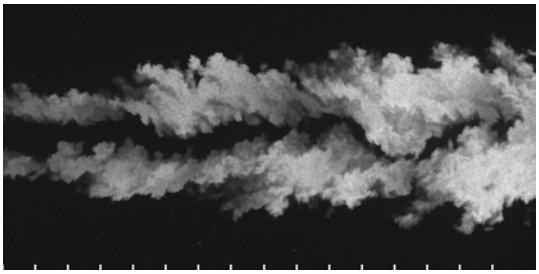 $f_F$ = 12 kHz, DC = 12% |
| 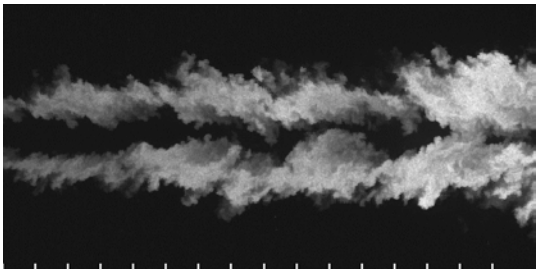 $f_F$ = 14 kHz, DC = 14% | 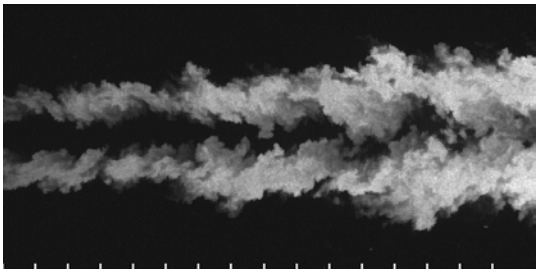 $f_F$ = 14 kHz, DC = 14% |
| 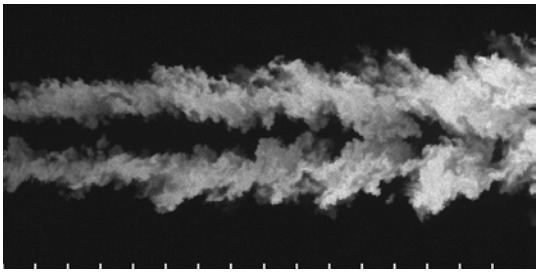 $f_F$ = 16 kHz, DC = 16% | 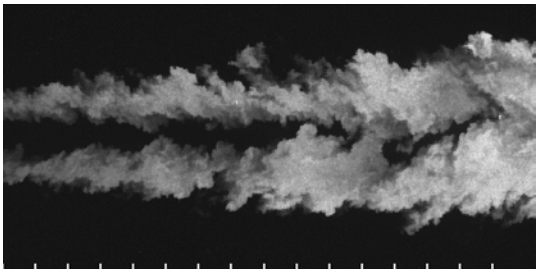 $f_F$ = 16 kHz, DC = 16% |

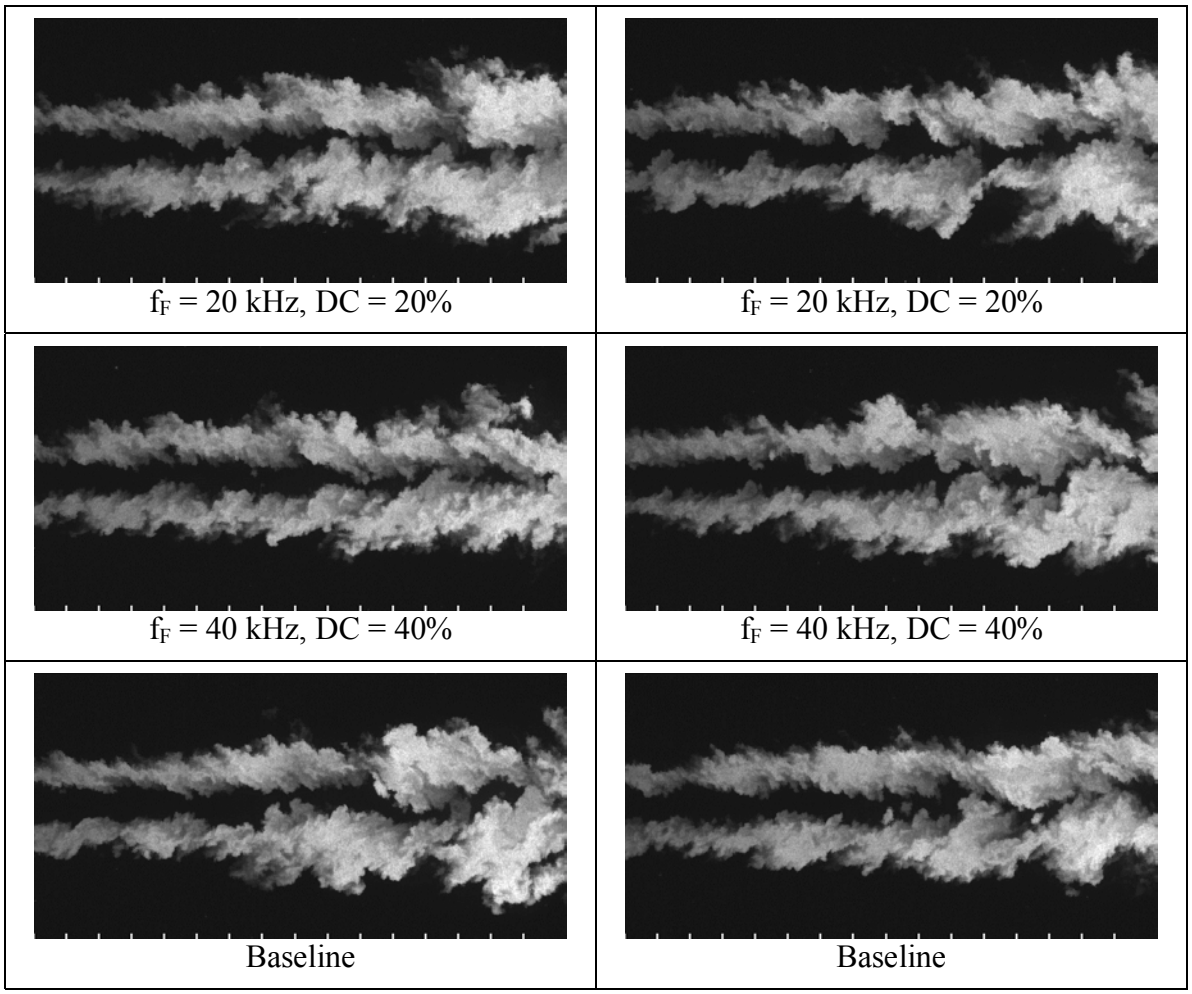


Figure 15. Instantaneous flow visualization images.

Figure 15 displays sample instantaneous images for each forcing case, showing the types of structures developed. Unlike the previous round of testing, the cases in which clear coherent structures can be seen, generally in the 6-8 kHz range, are not simply random images, but actually characteristic of the majority of individual images. For other test cases, the frequency of images displaying clear coherent structures is somewhat reduced. The images contained in Figure 15 for these cases display the optimum example of the formation of structures found within the data set for each case. This includes the baseline case, in which, as before, some structures can be seen without the effect of forcing. In general, structures are present within any flow regime. However,

operating outside of the ideally expanded flow regime will result in the presence of shock cells within the flow. Such shock cells can help to amplify and reinforce the development of structures, but this effect will have little influence once forcing is introduced. By forcing the jet, the structures become regular and patterned, allowing increased mixing and entrainment to become possible. As previously mentioned, the results found are similar to conclusions made by past researchers studying rectangular jets at the GDTL. The following figure displays acoustic data for a rectangular jet over a large frequency band. Instabilities within the flow appear as peaks in amplitude of sound pressure level recorded by the microphone, as was discussed in the previous analysis of stagnation pressure.

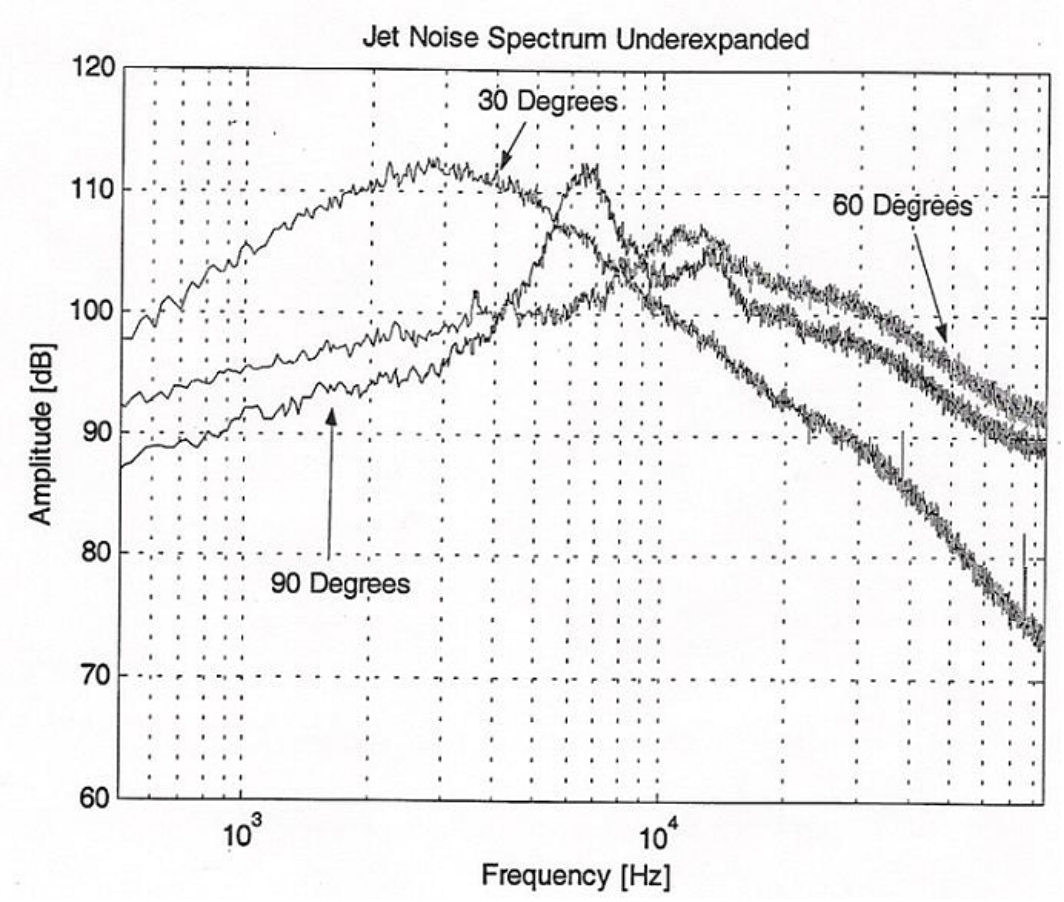


Figure 16. Broadband Shock Associated Noise for an underexpanded Mach 2 aspect ratio 3 rectangular nozzle (taken from Kerechanin 2000).

It should be noted that the most clear acoustic data is obtained from data recorded 90° relative to the nozzle exit. Moving to 30° causes the peak amplitudes to become lost due to turbulent mixing noise. It can be seen from this figure that the peak in amplitude can be found at 6500 Hz (Kerechanin 2000). This result closely correlates to those found in the present study. Further investigation of this frequency range will allow more definite conclusions to be made.

As an extension of the initial data set, the effect of duty cycle was also explored in this expanded set of tests. The primary concern is that the effect of forcing may be negatively affected as the duty cycle is further increased. Figure 16 provides a comparison of the forcing effects at 8 kHz for a variety of duty cycles. The effect of adjusting duty cycle in the 8 kHz forcing case had very little pronounced effects on the control of the jet. Lower duty cycles in the 4-8% range seem to produce more clearly defined structures than higher duty cycles, but all seem to produce obvious flow control patterns. In addition, the averaged images for each duty cycle are very similar, with only slight noticeable differences. The core of the jet appears slightly longer in the higher duty cycles cases when compared to lower duty cycles. The lowest duty cycle selected, 4%, corresponds to pulse duration of 5 μsec. This short of duration does not allow the actuator ample time to reach higher temperatures and sustain an arc, thereby reducing the effect of forcing. Increasing pulse duration allows more time for the arc to heat up and sustain, creating a more significant perturbation in the flow. This increased perturbation should, in theory, improve mixing enhancement. This can be seen above in the 16 and 32% cases where the structures developed become very pronounced. Previous work in the field of plasma actuators at the GDTL has shown that this temperature effect begins

to saturate as the pulse duration exceeds roughly 20 μsec (Utkin et. al. 2007). Despite this conclusion, forcing can still be observed in the 50% duty cycle case. It may therefore be concluded that although adjusting duty cycle at this frequency may have slight impacts on the character of structures developed, the system remains capable of controlling the jet even at higher duty cycles. This result may not be attainable at other frequencies, but for 8 kHz, the effect of forcing can be readily observed in all data sets.

| Average | Instantaneous |
|---|---|
| 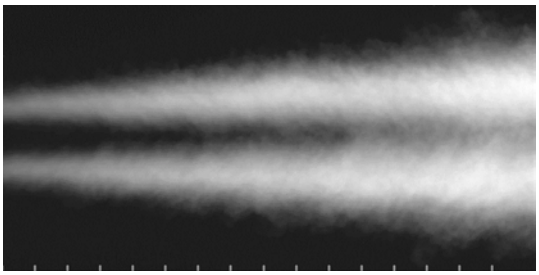 DC = 4% | 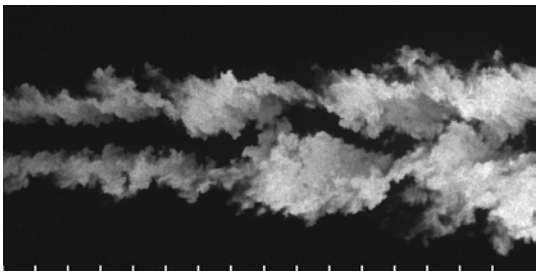 DC = 4% |
| 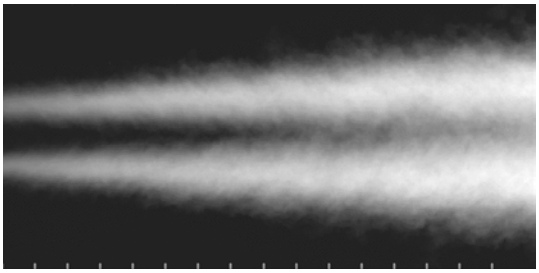 DC = 8% | 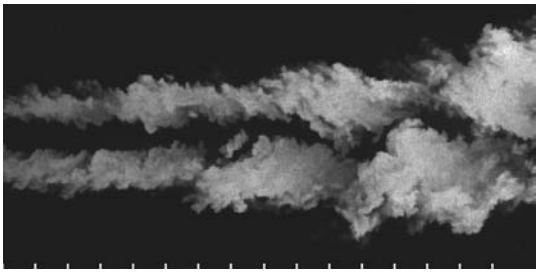 DC = 8% |
| 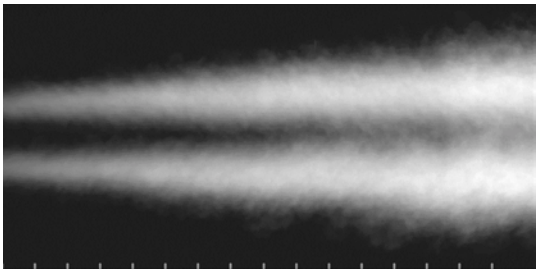 DC = 16% | 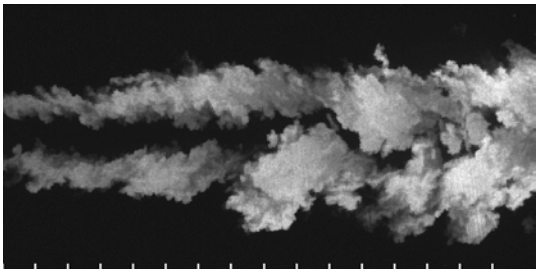 DC = 16% |

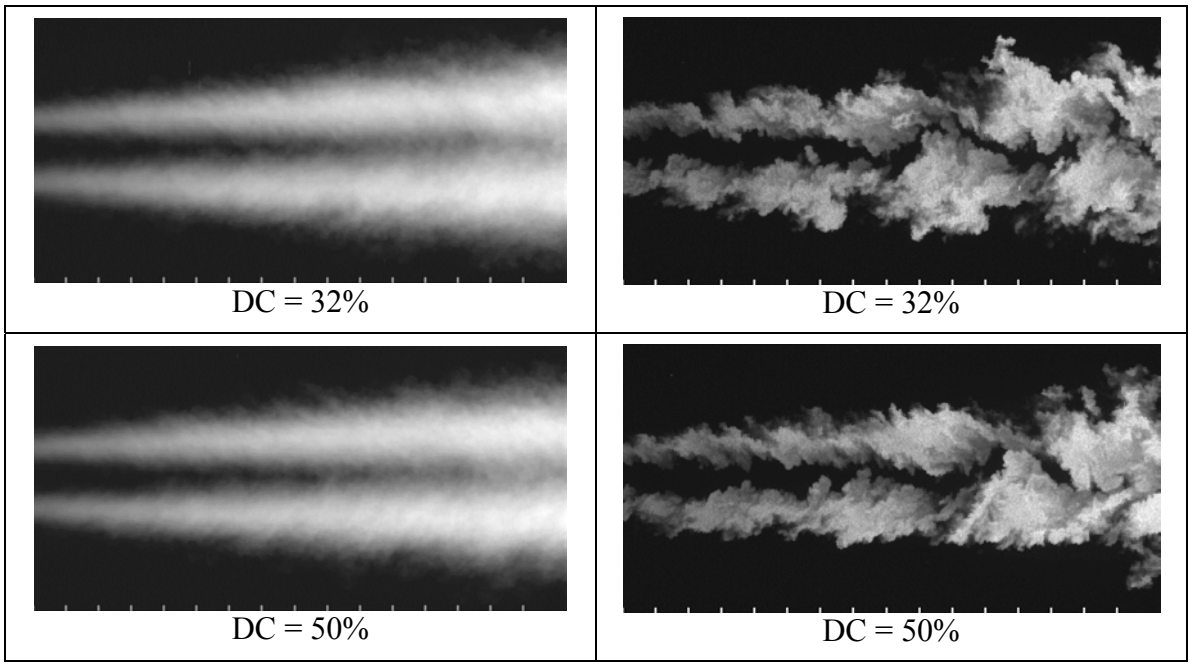

Figure 17. Effect of duty cycle on flow behavior for 8 kHz in flapping mode.

## 6. Summary and Future Work

To determine the effect of forcing on the development of turbulent structures in the flow exiting a rectangular nozzle, flow visualization techniques were employed. Flow visualization is a planar technique and relies on the scattering of laser light by condensed moisture from the ambient air entrained by the flow. A Mach 2.0 nozzle was selected in order to produce a temperature gradient significant enough to generate the required amount of condensation for flow visualization.

The flow was analyzed over a range of frequency and duty cycle combinations to provide a complete view of flow behavior in varying conditions. This was done in an attempt to find the ideal forcing conditions for maximum mixing enhancement. After initiating Mach 2.0 flow, a set of 71 images was recorded for each setup. These images were then averaged to provide an average picture of the flow behavior.

Initial particle image velocimetry (PIV) and flow visualization testing revealed some shortcomings of the experimental setup. The effects of both duty cycle and stagnation pressure were further investigated in an attempt to produce more accurate and reliable experimental results. Following this investigation, another battery of tests was conducted to provide more insight into the flow's response to actuation. This additional testing revealed obvious signs of control authority in several forcing frequencies and very prominently in the 6-8 kHz range. Further testing with PIV may confirm these results and provide more quantitative results to supplement the qualitative flow visualization results already obtained.

The extension of this study may not only explore other experimental methods, but may also be extended to other possible forms of control. Within the realm of Mach 2.0 flows, several possibilities for increased control authority exist. Methods of increasing the number of actuators used to excite the flow, or possibly changing the configuration of actuators may be explored in an attempt to improve the forcing of Mach 2.0 flows. Mach 2.0 flow is significantly colder than lower speed flows. Although this makes the effect of local heat perturbations more dramatic, the temperature of the flow may act as a sort of resistance to arcing, reducing the effect of forcing. The high flow speeds may also be blowing the arc downstream. Additional forms of testing such as pressure measurements may be conducted to help validate previously derived results. Lastly, the voltage of the actuators may be recorded and compared to the voltages at Mach 0.9 and 1.3 to determine the effect of flow speed on actuator characteristics. Beyond a rectangular jet, the effects of forcing a Mach 2.0 axisymmetric jet may also be explored. Researchers at the GDTL

have thoroughly studied both Mach 0.9 and 1.3 axisymmetric nozzles, but little work has been put forth to studying such high speed flows.

Subsequent flow visualization and PIV testing may also be conducted on a Mach 1.3 jet in order to allow more control of the jet and allow easier observation of flow behavior. If significant control authority can be established and effectively supported with future testing, other consequences of flow control, such as noise reduction, may be explored. Contrary to mixing enhancement, noise reduction may require varying degrees of mixing in order to achieve the desired results. This type of test can be readily validated through acoustical testing techniques similar to those employed throughout the study of stagnation pressure. This research has many potential applications, the possibilities of which will be investigated as part of the fulfillment of a Master of Science degree in the Department of Mechanical Engineering at The Ohio State University.

# REFERENCES


1. Anderson, J.D., Modern Compressible Flow with Historical Perspective, 3rd Edition, McGraw-Hill, New York City, NY, 2004.

2. Kerechanin, C.W., "The Effects of Nozzle Trailing Edge Modifications on the Acoustic Far Field of a Mach 2 Rectangular Jet," Master's Thesis, The Ohio State University, 2000.

3. Kim, J.-H. and Samimy, M., "Mixing Enhancement via Nozzle Trailing Edge Modifications in a High Speed Rectangular Jet," Physics in Fluids, Vol. 11, No. 9, pp. 2731-2742, 1999.

4. Kim, J.H., Samimy, M. and Erskine, W.R., "Mixing Enhancement with Minimal Thrust Loss in a High Speed Rectangular Jet," AIAA Paper 98-0696, January 1998.

5. Olsen, J.F., Rajagopalan, S., Antonia, R.A., "Jet column modes in both a plane jet and a passively modified plane jet subject to acoustic excitation," Experiments in Fluids, Vol. 35, pp.278-287, 2003.

6. Samimy, M., Adamovich, I., Kim, J.-H., Webb, B., Keshav, S., Utkin, Y., "Active Control of High Speed Jets Using Localized Arc Filament Plasma Actuators," AIAA Paper 2004-2130, June 2004.

7. Samimy, M., Adamovich, I., Webb, B., Kastner, J., Hileman, J., Kershav, S., Palm, P., "Development and Characterization of Plasma Actuators for High Speed Jet Control," Experiments in Fluids, Vol. 37, No. 4, pp.577-588, 2004.

8. Samimy, M., Kim, J.-H., Adamovich, I., Utikin, Y., and Kastner, J., "Toward Noise Mitigation in High Speed and High Reynolds Number Jets Using Plasma Actuators," to appear in *AIAA Journal*, 2007a.

9. Samimy, M., Kim, J.-H., Kastner, J., Adamovich, I., and Utikin, Y., "Active Control of High-Speed and High Reynolds Number Jets Using Plasma Actuators," to appear in *Journal of Fluid Mechanics*, 2007b.

10. Settles, G.S., *Schlieren and Shadowgraph Techniques*, Springer-Verlag, Berlin, Germany, 2001.

11. Utkin, Y.G., Keshav, S., Kim, J.-H., Kastner, J., Adamovich, I.V., and Samimy, M., "Development and Use of Localized Arc Filament Plasma Actuators For High-speed Flow Control", *Journal of Physics D: Applied Physics*, vol. 40, 2007, pp. 685-694.